

Gradient and Microfluidic Library Approaches to Polymer Interfaces*

Michael J. Fasolka, Christopher M. Stafford, and Kathryn L. Beers

Abstract We present an overview of research conducted at the National Institute of Standards and Technology aimed at developing and applying combinatorial and high-throughput measurement approaches to polymer surfaces, interfaces and thin films. Topics include (1) the generation of continuous gradient techniques for fabricating combinatorial libraries of film thickness, temperature, surface chemistry and polymer blend composition, (2) high-throughput measurement techniques for assessing the mechanical properties and adhesion of surfaces, interfaces and films, and (3) microfluidic approaches to synthesizing and analyzing libraries of interfacially-active polymer species.

Contents

- 1 Introduction: Surfaces and Interfaces in Polymer Science and Engineering
- 2 Continuous Gradient Library Techniques
- 3 Gradient Library Fabrication Methods and Application Examples
 - 3.1 Flow Coating: Polymer Film Thickness Gradients
 - 3.2 Gradient Hot Stage: Temperature Processing Libraries
 - 3.3 Surface Energy and Surface Chemistry Libraries
 - 3.4 Gradient Polymer Brush Libraries
 - 3.5 Polymer Blend Composition Gradients

M.J. Fasolka (✉), C.M. Stafford, and K.L. Beers
Materials Science and Engineering Laboratory, National Institute of Standards and Technology,
Gaithersburg, MD 20899, USA
e-mail: mfasolka@nist.gov; chris.stafford@nist.gov; kathryn.beers@nist.gov

* Official contribution of the National Institute of Standards and Technology; not subject to copyright in the United States. Certain commercial materials and equipment are identified in order to specify adequately experimental procedures. In no case does such identification imply recommendation or endorsement by the National Institute of Standards and Technology, nor does it imply that the items identified are necessarily the best available for the purpose.

- 4 High-Throughput Materials Testing: Surfaces, Interfaces, and Thin Films
 - 4.1 Thin Film Mechanical Properties
 - 4.2 Adhesion Testing
 - 5 High-Throughput Materials Synthesis and Solution Characterization: Microscale Approaches to Polymer Library Fabrication in Fluids
 - 5.1 Controlled Polymer Synthesis in Microchannels
 - 5.2 Characterization of Interfacially-Active Polymers in Microchannels
 - 6 Conclusions
- References

1 Introduction: Surfaces and Interfaces in Polymer Science and Engineering

The success of a huge range of polymer-based technologies, including advanced coatings and adhesives, electronics materials, complex fluid formulations and bio-materials, hinges on the ability to produce tailored polymer surfaces and interfaces. This is because surface and interfacial properties govern key aspects of product structure and performance, such as film and multilayer stability, mechanical reliability, adhesion, expression of functional moieties, component dispersion, and domain orientation, among others. Research dedicated to the understanding and engineering of these factors is extensive, and has proceeded for a number of decades; this is due to the fact that both the origins and effects of surface and interfacial properties are complex, depend upon a large number of variables, and can be difficult to predict. Both the importance and complexity of surface and interfacial science and engineering make them excellent targets for combinatorial and high-throughput approaches. Indeed, some of the first uses of these methods for polymeric materials systems focused on the formulation and performance testing of coatings [1], the behavior of which depend greatly on surface and interfacial effects.

Starting in the late 1990s, and continuing for the following 10 years, the National Institute of Standards and Technology (NIST) built and executed a research program that developed combinatorial methods aimed largely at addressing scientific and engineering challenges in polymer surfaces, interfaces and thin films. The NIST program, organized through the NIST Combinatorial Methods Center (NCCM, www.nist.gov/combi), concentrated on meeting two measurement-related needs in establishing combinatorial approaches for polymer surfaces and interfaces: the design and implementation of appropriate library fabrication and synthesis methods, and the development of high-throughput testing techniques to assess these libraries. This review surveys the research conducted through the NCCM with a focus on methodology, technique development and descriptions of supporting case studies in polymer surfaces, interfaces and films. The paper will start with a discussion of continuous gradient techniques, where NIST was a pioneer in polymer materials. The fabrication of gradient libraries for surfaces and interfaces will be considered next, including techniques for making continuous spreads in film thickness and composition, surface chemistry and surface energy and temperature. Application studies will include film stability and wetting, polymer self-assembly, polymer brush behavior

and measurements, biomaterials surface engineering. The next section will consider NIST-developed high-throughput approaches to measuring surface, interface and film performance properties. These include rapid measurement of film modulus, adhesion, and interfacial strength. Applications examples include mechanical testing of ultrathin film systems, ultrasoft polymers, engineering adhesives and relatively weak adhesive interactions. The final section will consider microfluidic and continuous microreactor approaches to polymer library fabrication and the high-throughput measurement of such systems. The primary focus will be on methods to produce systematic libraries of interfacially-active polymer species, such as block copolymers and macromolecular surfactants. Measurement applications will include microfluidic assessments of complex fluid structure, in particular solution self-assembly, and of fluid mixture properties such as interfacial tension.

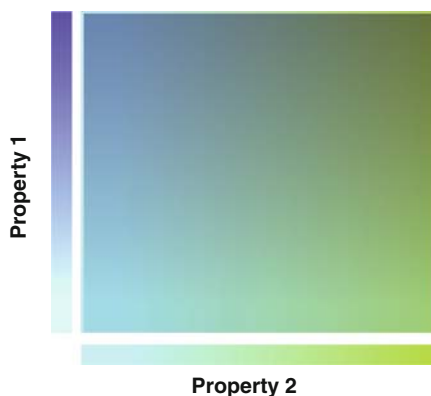
2 Continuous Gradient Library Techniques

A key challenge in combinatorial research is the creation of specimen *libraries* that exhibit a diversity of composition, processing conditions and other parameters over prescribed ranges. A common design for achieving this is the so-called “discrete” library, which consists of a large collection of individual sub-specimens. The main advantage of the discrete approach is the ability to incorporate a great number of different parameters in a single library – in this sense the design is versatile. However, since the library parameter space is divided into discrete sub-specimens, each with a single set of parameters, it is possible to “skip over” what may be important or interesting combinations of variables. Another disadvantage is that the fabrication of discrete libraries can depend upon complex, often expensive, equipment.

An alternate library design and fabrication strategy, and the one we focus on in this article, is the continuous gradient [2]. In this scheme, diversity is created by fabricating a specimen that gradually and continuously changes in a given parameter as a function of position (or as we will discuss later, as a function of time). Two or three continuous gradients can be combined in a single system. An illustration of a binary continuous gradient library can be seen in Fig. 1. Because they are continuous, and there are no “gaps” in the parameter space, gradient libraries present clear advantages for comprehensively examining and mapping the effect of the graded properties. For example, a binary gradient library exhibits every possible combination of the two graded parameters. As such, the gradient library design is excellent for mapping property correlation, and for identifying optimal conditions or critical phenomena that may exist only over a small range or at a specific parameter combination. Indeed, for materials scientists, gradient libraries can be a natural experimental design, since they are quite similar to the phase diagrams they use to represent two and three parameter systems.

A key aspect of gradient libraries is that they reside on a single substrate, and this has several advantages. Foremost, gradient libraries yield an entire set of systematic results from a single compound experiment. In this sense, they are “self-reporting”,

Fig. 1 Illustration of a 2D continuous gradient combinatorial library that exhibits gradual and systematic changes in two variables



meaning that they can illuminate trends and express key results without extensive analysis (our example of a single specimen phase diagram, discussed below, will illustrate this point). Moreover, because the entire library undergoes identical processing, “sample to sample” errors (inherent to combining single measurements on individual specimens) can be reduced. Finally, gradient libraries can often be produced with simple, inexpensive equipment, which makes this approach accessible to academic laboratories and small companies.

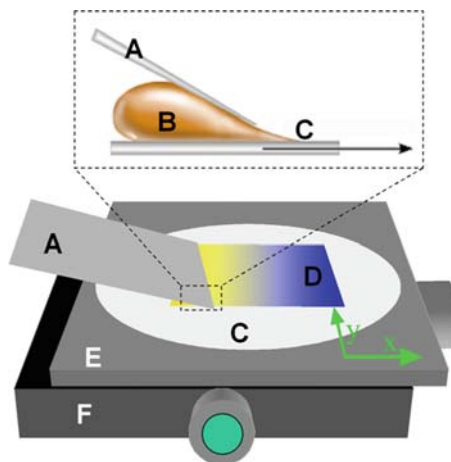
3 Gradient Library Fabrication Methods and Application Examples

Gradient libraries generally assume a planar form, and are supported by a substrate. Often the library is a material deposited onto the substrate as a thin coating, or it can be achieved through chemical modification of the substrate itself. This geometry naturally gears gradient libraries for the examination of thin films, coatings and of the interfacial properties that govern these systems. At NIST, our goal was to create a suite of gradient library fabrication technologies that would be a combinatorial platform for examining polymer thin film physics phenomena including wetting and stability, blend phase behavior, self-assembly, and confinement effects.

3.1 Flow Coating: Polymer Film Thickness Gradients

Film thickness can govern the morphology, stability, and surface-chemical expression of polymeric thin films. NIST researchers developed a process for producing gradients, termed flow coating, which is a modified blade-casting technique [3–5]. Flow coater instrumentation and the flow coating process are illustrated in Fig. 2. To create the library, a dilute solution of polymer in solvent (1–5% mass fraction) is injected into the gap between a doctor blade positioned over a flat substrate

Fig. 2 Flow coater for creating polymer gradient thickness libraries: **A** doctor blade; **B** polymer solution; **C** substrate; **D** thickness library; **E** x -translation stage; **F** y -translation stage (for characterization). (Reproduced with permission from [13])



(e.g., silicon wafer) mounted on a computer-controlled translation stage. The stage/substrate is accelerated beneath the stationary blade in the x -direction as shown in Fig. 2. As the stage accelerates, increasing amounts of solution are deposited along the substrate. Subsequent solvent evaporation results in a gradient polymer film thickness library. As demonstrated by Stafford et al. [5], the range and slope of the thickness gradient can be precisely tuned through the stage velocity profile, solution concentration, and gap height.

Films produced via flow coating can be from ≈ 20 to ≈ 1 mm in thickness. A typical library will double in thickness over about 40 mm in length. In the range of 50–600 nm, libraries exhibit constant slopes of ≈ 1 – 10 nm mm^{-1} , depending upon processing parameters. In the NIST instrument, thickness gradients are characterized via spot interferometry. In this scheme, stacked translation stages (including the stage used to produce the specimen) raster the sample beneath the interferometer footprint, resulting in a 2D map of film thickness. With careful instrument construction and operation [5], thickness libraries created via flow coating are linear along the x -direction, and level along the y -direction (to about 3% of the average film thickness at a point x), but 2D thickness characterization may be necessary for the most quantitative combinatorial analysis.

When used with polymer solutions in the few percent by mass range, the flow coating instrument creates films that are comparable in thickness and roughness to those created by spin casting, i.e. ranging from ≈ 10 to 500 nm thickness, with root-mean-squared roughness ≤ 1 nm. However, it should be noted that spin casting typically drives solvent from the system much faster than with flow coating and this can affect the film morphology [6]. Recently, de Gans and coworkers [7] demonstrated a “sector” spin casting technique for creating discrete polymer film libraries. In this technique, a metal template is used to divide a round substrate into pie-slice shaped sectors, into which a series of polymer solutions can be deposited and cast. By varying spin speed and solution concentration, a discrete film thickness library could be built; moreover, the method can be used to cast discrete compositional libraries of, for example, polymer blends. Another route for discrete

film library fabrication is ink jetting, which has been explored by several groups [8–11]. As with sector spin coating, this technique can be used to create compositional spreads. However, ink jetting does not seem to offer the deposition control necessary to produce well-behaved thickness libraries, since ink jetted spots typically exhibit irregular thickness profiles due to “coffee ring” and other drying effects.

3.2 Gradient Hot Stage: Temperature Processing Libraries

Polymer thin film properties are often governed or modified by high-temperature annealing and processing, with most phenomena (phase transitions, dewetting, melting etc.) occurring below about 300°C. Accordingly, a temperature gradient with modest range can create a useful map of the effect of temperature on polymer film libraries. This concept has been examined in the literature [12], and in past decades several companies have used this concept to produce gradient hot-stages for applications that include melting-point determination. In recent years, NIST researchers designed a gradient hotstage with the aim of producing a flexible instrument that could accommodate libraries of various lengths, and that had a tunable temperature profile [13–15].

Figure 3 illustrates the NIST gradient hot stage design. The instrument consists of an aluminum sample platen (10 cm × 15 cm × 0.5 cm) perforated with two slots (along x). Two aluminum blocks, fitted with heating/cooling channels, are attached to the bottom of the platen through the slots. This set-up enables control of the inter-block distance, which allows the positions of the heating/cooling sources to be matched with length of the specimen library. The blocks hold cylindrical heating cartridges or accommodate plumbing for fluid-mediated cooling.

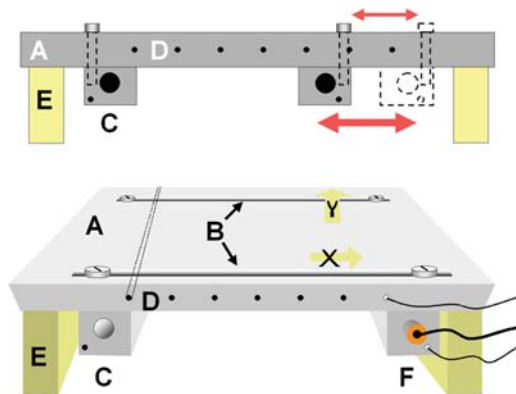


Fig. 3 NCMC gradient hot stage: **A** sample platen; **B** slots for mounting/positioning of heating/cooling blocks; **C** block with channel for heating/cooling element with thermocouple ports for temperature control; **D** thermocouple ports for gradient characterization; **E** ceramic blocks for mounting hot stage; **F** block with cylindrical heating element and thermocouple installed. (Reproduced with permission from [13])

Proportional–integral–derivative (PID) temperature controllers maintain the block temperatures, measured through integrated thermocouples. By heating (or cooling) each block to a constant temperature, a temperature gradient is produced across the platen. Ceramic supports insulate the device, so it can be mounted on, for example, a microscope translation stage or other observation instrument. The range and slope of the temperature gradient are tailored through the block distance and the temperatures of the heating/cooling sources. Remarkably, for modest temperature ranges ($\approx 200^\circ\text{C}$) the temperature profile is linear [14] along the gradient (x -direction), and level perpendicular to the gradient (y -direction), so measurements of the temperatures at the ends stage are sufficient to characterize the gradient. However, in the NIST instrument, thermocouple ports drilled into the platen edge enable temperature measurements along the gradient. Using this device, typical temperature gradients span intervals of about 100°C over a total range of room temperature to about 300°C .

In conjunction with both in situ and ex situ automated measurements, a gradient hot stage can be a powerful tool for examining the role of temperature on film microstructure, morphology development kinetics, phase transitions and performance. For example, Lucas et al. [15] recently used the NIST gradient hot stage to map the effect of temperature processing on the structure and performance of organic semiconductor films. In this study, polythiophene thin films were annealed on a temperature gradient that crossed the bulk liquid-crystal transition of the material. The resulting film library exhibited a range of morphologies across this transition, which could be observed via atomic force microscopy (AFM) conducted along the library. In addition, this team employed an automated probe station to measure the field effect mobility along the specimen, resulting in a map of the material's electronic performance. With this strategy, and using a single specimen, the authors were able both to identify the annealing temperature that gave optimal performance, and to determine how the mobility was correlated with film microstructure. In a similar scheme, Eidelman and coworkers [16] used the gradient hot stage in conjunction with automated Fourier transform infrared (FTIR) microspectroscopy and high-throughput adhesion testing to map correlations between curing temperature, degree of curing and surface tack of model epoxy adhesive formulations. By combining a temperature gradient, flow coating, and automated optical microscopy, Beers et al. [14] were able to examine simultaneously the roles of temperature and thickness on the crystallization rate of isotactic polystyrene. In this study, flow coating was used to create a film thickness library of the polymer, which was placed orthogonal to a temperature gradient. Automated micrographs were collected across a grid of points on the library, each of which represented a different combination of thickness and crystallization temperature. Time sequences of crystallite growth were built by repeating the cycle of micrograph acquisition over a few hours, which yielded a 2D map of crystallization rates as a function of thickness and temperature. In addition, analysis of the library via AFM and optical microscopy allowed the researchers to observe several thickness dependent transitions in crystallite morphology.

3.3 Surface Energy and Surface Chemistry Libraries

A key factor that governs the behavior of polymer thin films is its interaction with an underlying substrate. In combination with other factors, surface energy and chemistry of the substrate can cause film instability and dewetting, shifts in thermodynamic and morphological transitions, changes in nano-domain orientation, and modifications in the expression of chemical moieties at the substrate/film interface and free film surface. In addition, surface energy/chemistry can affect the mobility, growth and morphology of adsorbed cells in biological systems. NIST researchers have developed two main strategies for creating libraries of substrate surface energy/chemistry, which are useful for screening the effect of this factor on the behavior of overlying films and other materials. First, we will discuss the use of graded ultraviolet light–ozone (UV–ozone) exposure to fabricate surface energy libraries, and some of the combinatorial studies that resulted from this capability. Then, in the next section, we will consider more sophisticated surface chemistry libraries fabricated through surface-initiated polymerization, and the use of these graded polymer “brush” layers for high-throughput analysis.

It is well known that exposure of organic molecules to ozone generated from ultraviolet–light (UV–ozone) can cause a variety of oxidative reactions – this is the basis of UV–ozone surface cleaning devices. For alkyl chain molecules, UV–ozonolysis leads first to the formation of oxygen containing moieties, typically starting at the chain ends, with the eventual consumptive oxidation of the molecules at long exposures. Since the degree of oxidation is dependent upon the UV–ozone dosage, this process can be harnessed to create a gradient surface energy library. There are several ways to create the gradient in UV–ozone exposure needed to accomplish such libraries. In one strategy, NIST researchers [17, 18] used a UV–ozone flood source (185 and 254 nm light) to illuminate a planar substrate through a graded neutral density filter, which systematically decreased the amount of transmitted light as a function of position. The substrate was a native oxide-terminated silicon wafer, treated with a self-assembled monolayer (SAM) of *n*-octyldimethylchlorosilane (ODS).

As shown in Fig. 4a for an ODS treated substrate, the library exhibits a systematic change in water contact angle along its length. Roberson and coworkers [17] also used more sophisticated contact angle measurements to yield the polar and dispersive parts of the total surface energy (Fig. 4b). These measurements demonstrate that the UV–ozone treatment changes the polar part of the surface energy, while leaving the dispersive part relatively unchanged. Time-of-flight secondary ion mass spectrometry measurements across the library show that the UV–ozonolysis gradually imparts the hydrophobic, methyl-terminated, ODS SAM layer with a variety of oxygen containing end-groups, but these were primarily –COOH terminated species. The growing number of –COOH terminated species along the library results in its increasing hydrophilicity (i.e. lower water contact angles) as shown in Fig. 4.

More recently, NIST researchers [13, 19] developed a device to more precisely generate surface energy libraries using OV-ozonolysis. Pictured in Fig. 5, this device achieves graded UV–ozonolysis through a computer-driven translation stage,

Fig. 4 Water contact angle data (a) and surface energy data (b) from a surface energy library produced through the graded UV–ozonolysis of an ODS self-assembled monolayer on silicon. (Reproduced with permission from [17])

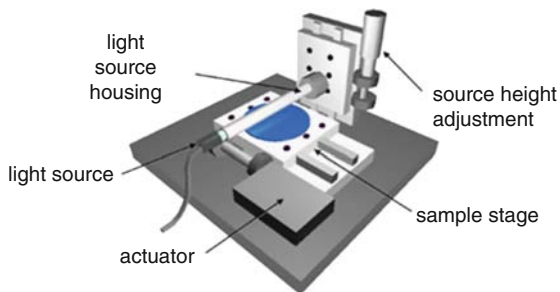
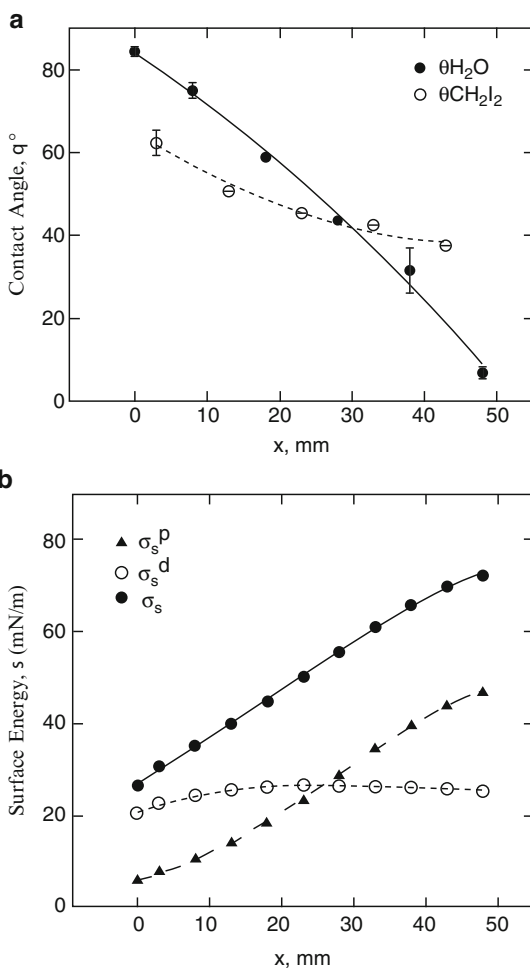


Fig. 5 Illustration of NIST Gradient UV–Ozone device for generating surface energy libraries on substrates functionalized with hydrophobic SAM species. The sample stage accelerates the specimen (blue) beneath a slit-source of UV light. (Reproduced with permission from [12])

which accelerates the silanized substrate beneath a 185 nm/254 nm UV wand-source projected through a 2 mm-wide slit aperture cut into the cylindrical lamp housing. The gap between the aperture and the substrate is controlled through a micro-positioner incorporated into the fixed lamp mount. Using these exposure-mediated methods on ODS treated silicon, surface energy gradients can span any interval between 20 mJm^{-2} and 75 mJm^{-2} , over a tunable length of 1–5 cm. Water contact angles typically span 100° to less than 10° .

The main advantage of this approach is the ability to determine the stage acceleration profile via computer control [19]. As opposed to a graded density filter (which represents a single static exposure “function”) any mathematical function can be fed into the stage motion routine. This enables users to tune the length, steepness and shape of the surface energy profile in the library. Indeed, this sort of control can be used to create a well-behaved surface energy gradient profile, which can ease its application in combinatorial screening. For example, this capability can be used to create libraries that have a linear surface energy gradient, rather than the sigmoidal surface energy profile that results from a linear exposure function (as in Fig. 4). In this sense, this method also presents an advantage over techniques for creating surface chemistry gradients via diffusion mediated deposition of SAM species (see for example [20–22]), since these techniques also result in a steep, sigmoidal gradient profile. However, diffusion techniques and controlled immersion methods [23] offer the possibility of creating more chemically diverse mixed SAM gradient libraries via the simultaneous graded deposition of two SAM species [24, 25], or through a backfill sequence [26, 27].

The graded UV–ozonolysis approach to surface energy library fabrication is a powerful tool for examining the role of substrate-polymer interactions on film phenomena such as dewetting and block copolymer self-assembly. Ashley et al. [28], used this approach to determine the surface energy dependence of the stability and dewetted morphology of polystyrene films. In conjunction with an orthogonal temperature gradient, and automated optical microscopy, this team was rapidly able to map the dewetting behavior of five polystyrene specimens that varied in their molecular mass. The library approach enabled the team to observe the surface energy and temperature bounding conditions for film stability, since the dewetted portions of the film could be easily screened. Indeed, the authors discovered that, for the range of molecular mass they considered, these boundary conditions could be collapsed to a common “master curve”, which suggests that a universal surface energy and temperature-dependent dewetting behavior is exhibited by this system.

A number of researchers have used surface energy libraries to examine the self-assembly of block copolymer species in thin films. It is well known that substrate-block interactions can govern the orientation, wetting symmetry and even the pattern motif of self-assembled domains in block copolymer films [29]. A simple illustration of these effects in diblock copolymer films is shown schematically in Fig. 6. However, for most block copolymer systems the exact surface energy conditions needed to control these effects are unknown, and for many applications of self-assembly (e.g., nanolithography) such control is essential.

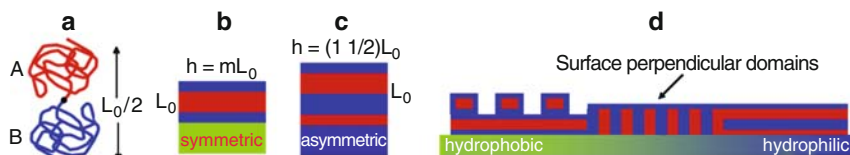


Fig. 6 Illustration of surface energy effects on the self-assembly of thin films of volume symmetric diblock copolymer (a). Sections b and c show surface-parallel block domains orientation that occur when one block preferentially wets the substrate. Symmetric wetting (b) occurs when the substrate and free surface favor interactions with one block B, which is more hydrophobic. Asymmetric wetting (c) occurs when blocks A and B are favored by the substrate and free surface, respectively. For some systems, a “neutral” substrate surface energy, which favors neither block, results in a self-assembled domains oriented perpendicular to the film plane (d). L_0 is the equilibrium length-scale of pattern formation in the diblock system

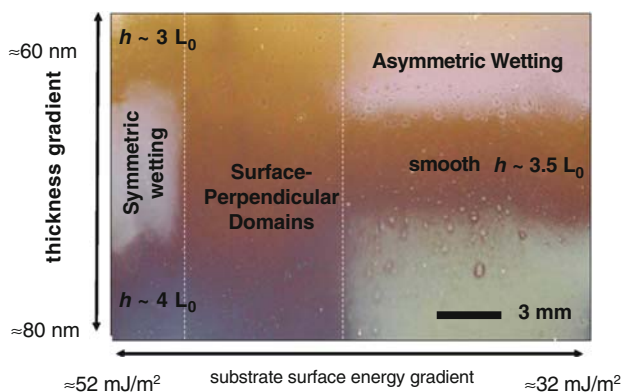


Fig. 7 2D thickness-surface energy gradient library for mapping the effects of these parameters on the self-assembly of PS-b-PMMA block copolymer thin films. See text for a full description. L_0 is the equilibrium self-assembly period and h is the film thickness. Dashed white lines delineate the “neutral” surface energy region, which exhibits nanostructures oriented perpendicular to the substrate plane. (Derived from [18] with permission)

To address this problem, Smith and coworkers [18] combined flow coating and surface energy gradients to generate a single specimen that maps the effects of film thickness and surface interactions on the self-assembly of polystyrene-b-poly(methyl methacrylate) (PS-b-PMMA) thin films. This thin film library is shown in Fig. 7. As demonstrated by this photograph of the specimen, the formation of microscopic “island and hole” structures, which make areas of the film hazy, make the library “self-reporting” via simple visual inspection. These surface features only occur when the block domains are oriented parallel to the surface, and they have a specific thickness-dependence, i.e. they disappear when the film thickness is an exact integral (or $n + 1/2$ integral) of the equilibrium period (L_0) of the diblock self-assembly. Examination of the thickness-dependence enabled the authors to determine the wetting symmetry of the surface-parallel self-assembly in these areas (see Fig. 6 caption). Moreover, the range of “neutral” substrate

surface energy is clearly indicated by the vertical band of film in which there is a lack of hazy bands regardless of film thickness. This range of surface energy causes the domains to orient perpendicular to the film surface. In this study, Smith et al. used the method to examine rapidly the molecular mass dependence of the width of the neutral surface region, which is a measurement of the diblock's susceptibility to surface interactions. Moreover, a separate gradient analysis of the thickness-dependence of the "island and hole" structures in diblock films yielded observations of a new labyrinthine form of this surface phenomenon [30].

Other teams used the surface energy gradient approach to examine the more complex thin film self-assembly of three component triblock copolymers. For example, Ludwigs et al. [31] used the technique to screen for surface energy dependent morphological shifts in a PS-*b*-poly(vinylpyridine)-*b*-poly(*tert*-butyl methacrylate) triblock films. Remarkably, in a single library experiment, the authors observed that the system exhibited a perforated lamella motif in thin films regardless of the substrate surface energy. This finding has interesting implications for lithographic applications, since it indicates that this laterally structured nanopattern can be formed on almost any smooth substrate material. More recently, Epps and coworkers [32] performed a similar study of a polyisoprene-*b*-PS-*b*-poly(ethylene oxide) triblock films. As with the work of Ludwigs et al., this examination showed that, regardless of the surface energy of the substrate, the triblock formed a different morphology in thin films to that in the bulk, in this case three-layered surface-parallel lamella. However, the authors observed that, at long annealing times, the lamellar films unexpectedly dewet the substrate over a specific range of surface energy. Using a high-throughput technique developed to pluck film specimens from the library [33] the team could examine the buried film–substrate interface via automated X-ray surface spectroscopy methods. Using this data, the unexpected phenomenon was determined to be a form of surface energy dependent autophobic dewetting that had not been observed previously. In both of these studies, it is unlikely that these key observations could have been made as readily without the comprehensive scope of the gradient library approach.

The UV–ozone gradient exposure approach can also be used to fabricate more complex libraries. For example, Julthongpipit and coworkers [34, 35] employed the technique to create libraries that exhibit a graded chemical micropattern. As illustrated in Fig. 8, these combinatorial test substrates consist of a pattern of micron-scale lines that exhibit a continuous gradient in surface energy differences against a constant surface energy matrix. On one end of the specimen the lines are strongly hydrophobic while the substrate matrix is hydrophilic SiO₂. The lines become increasingly more hydrophobic towards the other end of the library until they are chemically indistinguishable from the matrix. The library is fabricated through a vapor-mediated soft lithography [34] of an ODS SAM which is then treated to a graded UV–ozonolysis with the device shown in Fig. 5. The library design includes two calibration strips that express the changing and static surface energy of the SAM pattern lines and matrix respectively. Accordingly, the surface energy differences along the patterned region can be determined by contact angle measurements along the calibration strips.

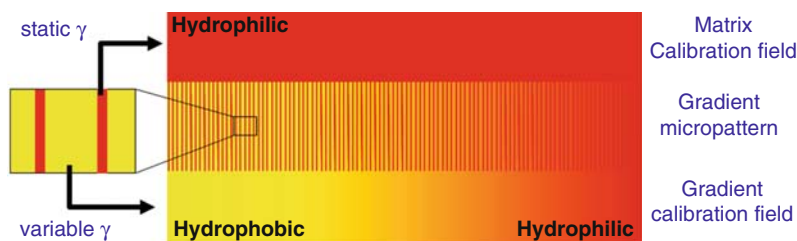


Fig. 8 Illustration of a gradient micropattern library. The central band of the library exhibits a micropattern that gradually changes the chemical differences between the striped domains and the matrix until the surface is chemically homogeneous. The bands on the top and bottom of the library are the calibration fields for static matrix and gradient respectively. γ is surface energy

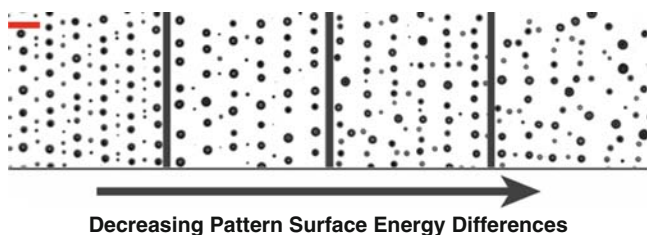


Fig. 9 Optical micrographs of dewetted polystyrene droplets collected from points along a chemical gradient library. Scale bar (red) is approximately $20\mu\text{m}$. As discussed in the text, this library was used to examine the transition between pattern directed dewetting (left micrographs) and isotropic dewetting from a homogeneous surface (right micrograph). (Reproduced with permission from [35])

The gradient micropattern library is a unique combinatorial tool for examining the effects of substrate chemical heterogeneity on surface, interface and thin film phenomenon. Julthongpiput et al. [35] recently demonstrated this library as a means to determine how the chemical differences between the stripes can drive the rupture, dewetting and patterning of overlying polystyrene thin films. In this study, automated optical microscopy was employed to collect 1,700 contiguous optical micrographs of polystyrene droplets that formed as a result of dewetting from the gradient micropattern substrate. A small, representative selection of these images is shown in Fig. 9. Automated image analysis was used to examine the droplet arrangements, in particular their registry with the underlying pattern. Through this data, the team could determine the range of surface energy differences that resulted in “pattern directed” dewetting, i.e. film instability, rupture and droplet alignment caused by the underlying stripes. In particular, the library showed that chemical differences between 14mJm^{-2} and 20mJm^{-2} resulted in the best droplet alignment. Moreover, the library data showed that when the pattern chemical differences dropped below 7mJm^{-2} , the droplets had an isotropic arrangement indicative of dewetting from a homogeneous surface. This key observation, which precisely illuminates the minimum surface-chemical heterogeneity needed to induce film dewetting, would have been very difficult to make using traditional “single specimen” methods.

Another variation and application of the UV–ozone surface energy library was demonstrated recently by Gallant et al. [36]. In this work, the surface energy library is used as a facile platform for further modification by the “click” chemistry [37] route. In particular, the graded –COOH terminated SAM molecules produced by the UV–ozonolysis are reacted with a bifunctional cross-linker terminated with both amino and alkyne functional groups. The result is a library that has an increasing density of SAM chains with alkyne functionality. Through the click chemistry scheme, the alkyne can react with a huge variety of azido-derivatized biofunctional molecules. Accordingly, this versatile scheme enables continuous gradients in the grafting density of a number of bioactive species. The authors demonstrated this approach by creating a library that continuously varied the concentration of surface-bound RGD peptide molecules. This gradient was used to measure the effect of RGD density on cell adhesion and morphology. Using automated fluorescence microscopy, the team was able to measure cell behavior under a huge number of RGD concentrations, and determine the RGD densities that resulted in the most number of adhered cells, and the most extensive cell spreading. Such data is critical when designing surfaces for cell scaffolds and other biomaterials applications.

The general approach of graded radiation exposure can also be used to examine light driven processes such as photopolymerization [19]. For example, Lin-Gibson and coworkers used this library technique to examine structure-property relationships in photopolymerized dimethacrylate networks [38] and to screen the mechanical and biocompatibility performance of photopolymerized dental resins [39]. In another set of recent studies, Johnson and coworkers combined graded light exposure with temperature and composition gradients to map and model the photopolymerization kinetics of acrylates, thiolenes and a series of co-monomer systems [40–42].

3.4 Gradient Polymer Brush Libraries

While UV–ozone-generated surface energy libraries are simple to implement, they pose limitations in terms of both stability and chemical diversity. Chlorosilane SAMs modified via UV–ozonolysis are susceptible to degradation under light exposure, oxygen, humidity, and high-temperature, and thus must be used within a few hours of fabrication. Moreover, without further modification (as in the example from Gallant and coworkers above), this route generally results in a gradient only between –CH₃ and –COOH functionalities. In order to create more robust and diverse surface chemistry gradients, NIST researchers turned to surface-initiated polymerization (SIP) techniques [43,44] to create libraries of grafted polymer “brushes” that would systematically change in their molecular composition and architecture. In this endeavor, the pioneering work of Genzer and coworkers [45–48] provided examples to build upon, including the creation of gradient libraries of polymer brush length and grafting density.

SIP involves the growth of a polymer chain from an initiator moiety that has been covalently tethered to a surface. The advent of this reaction approach, along

with advances in polymer synthesis routes, have enabled the creation of densely packed polymer “brush” layers that can exhibit a huge variety of macromolecular compositions, architectures and functional groups [49, 50]. Because this covalently bound layer can result in overlapping polymer coils, surface coverage is enhanced. Moreover, some polymer types and architectures offer the possibility of generating surfaces with advanced functionality including, chemical switching, reversible wetting and bioactivity [51, 52]. The potential chemical diversity and technological promise of polymer brushes present opportunities for new library fabrication methods, and for applications of combinatorial techniques. In the following passages, we will discuss how NIST researchers examined both of these opportunities.

SIP-driven polymer brush library fabrication leverages the fact that the polymerization initiation species are permanently bound to the substrate. Since the initiators are tethered, controlled delivery of monomer solution to different areas of the substrate results in a grafted polymer library. In NIST work, initiators bound via chlorosilane SAMs to silicon substrates were suitable for conducting controlled atom transfer radical polymerization (ATRP) [53] and traditional UV free radical polymerization [54, 55]. Suitable monomers are delivered in solution to the surface via microfluidic channels, which enables control over both the monomer solution composition and the time in which the solution is in contact with the initiating groups. After the polymerization is complete, the microchannel is removed from the substrate (or vice versa). This fabrication scheme, termed microchannel confined SIP (μ -SIP), is shown in Fig. 10. In these illustrations, and in the examples discussed below, the microchannels above the substrate are approximately 1 cm wide, 5 cm long, and 300–500 μm high.

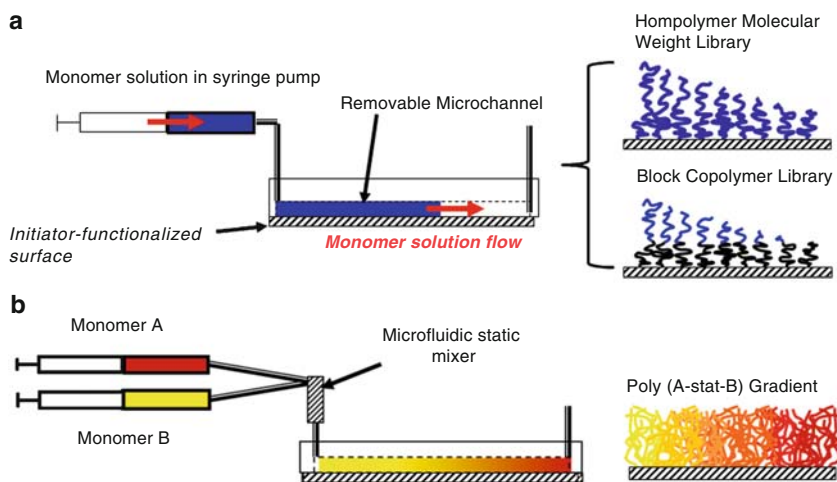


Fig. 10 Illustrations of the microchannel confined surface-initiated polymerization (μ -SIP) route for producing gradient polymer brush libraries: **a** route for making polymer molecular weight and block copolymer libraries; **b** route for making statistical copolymer libraries. *Red arrows* show the flow of monomer solution from a syringe pump used to gradually fill the microchannel. See text for details

As illustrated in Fig. 10a, and described by Xu and coworkers [56], the most basic implementation of μ -SIP involves a gradual filling of the microchannel with monomer solution under polymerization conditions. Depending on the rate of the polymerization and the desired library design, the microchannel is filled using a computer-controlled syringe over 5–40 min. Accordingly, beginning from the microchannel feed, the substrate is exposed to the monomer solution for a decreasing length of time, which is equivalent to a decreasing polymerization period along the library. This process results in a grafted polymer library that gradually decreases in its molecular mass and is evidenced by decreasing film thickness, as demonstrated in Fig. 11a for a poly(*N,N*-dimethylaminoethyl methacrylate) (PDMAEMA) homopolymer [56]. If a living polymerization route (such as ATRP) is used to grow constant-length polymers from the substrate, a similar process can be employed with a second monomer solution to fabricate a block copolymer library in which the second block gradually decreases in its length. As shown in Fig. 11b, Xu and coworkers [57,58] demonstrated this technique by fabricating a series of grafted block copolymer libraries consisting of poly(*n*-butyl methacrylate) (PnBMA) and PDMAEMA. An application of these libraries will be discussed below. A variation of this approach can be used to create a gradient in polymer grafting density. As demonstrated by Mei et al. [59], this involves creating a gradient in surface-bound initiator concentration, which is achieved by gradually introducing initiator-SAM solution along the substrate. Subsequent immersion in the monomer solution results in a library that systematically varies the lateral spacing of tethered polymer chains. A similar technique for creating grafting density libraries has been published by Wu and coworkers [47].

As illustrated in Fig. 10b, a more sophisticated *statistical copolymer* gradient library can also be fabricated through the μ -SIP method [60]. The key to this library is a microfluidic mixer, positioned between two monomer solution feeds and the microchannel. The mixer serves to combine a ramped flow of these solutions in which the relative amount of one solution is decreased and the other increased over time. The result of this ramped input is that the microchannel is filled with a gradient monomer solution composition. Because of the narrow height dimensions of the channel, cross diffusion of the monomers is suppressed, and the solution gradient can persist over a few hours. Accordingly, during a period of polymerization, the monomer concentration profile is transferred to grafted polymer chains on the substrate. The resulting statistical copolymer brush gradient gradually changes from nearly 100% of one monomer to 100% of the other along the library. Composition data from a PnBMA-*s*-PDMAEMA statistical copolymer library, collected via near edge X-ray absorption fine structure (NEXAFS) spectroscopy, can be seen in Fig. 11c [60]. This achievement is exciting since it represents a way of producing surface chemistry libraries that exhibit both the reliability and enhanced coverage of covalently bound polymer brushes, and the potential for creating chemical gradients that exhibit the extensive chemical and architectural functionality available from advanced polymerization routes. In addition, a key feature of grafted statistical copolymers is that they present stable and intimate blends of disparate chemical species. Since the different monomers are bound within the same chains, the system

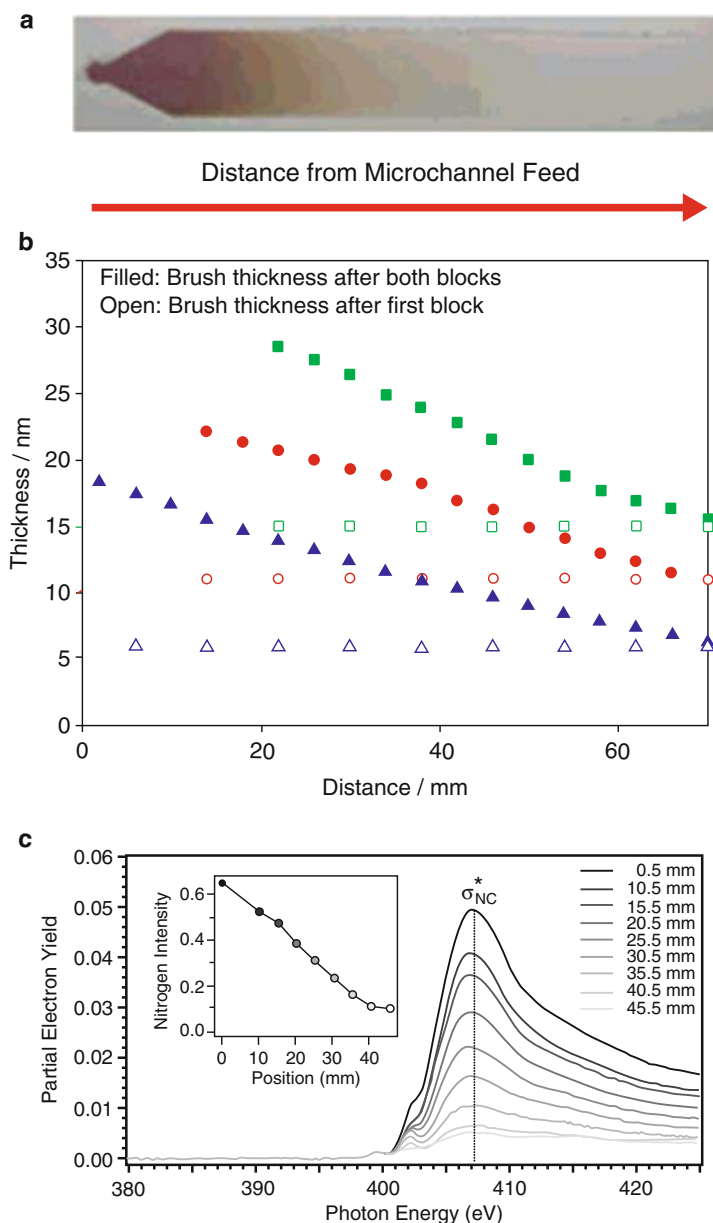


Fig. 11 Data from polymer brush libraries generated by μ -SIP: **a** photograph of molecular weight gradient of grafted PDMAEMA. The entire library is approximately 50 mm long. The brush thickness ranges from approximately 60 to 0 nm from left to right. (Reproduced with permission from [56]); **b** thickness data (ellipsometry) from a PnBMA-b-PDMAEMA block copolymer library after the growth of the PnBMA block (*open symbols*) and the PDMAEMA block (*closed symbols*). (Reproduced with permission from [58]); **c** NEXAFS data along PnBMA-s-PDMAEMA statistical copolymer gradient library. The decreasing nitrogen edge electron intensity signal demonstrates that the DMAEMA segment content of the statistical copolymer systematically decreases along the library. (Reproduced with permission from [60])

will not undergo lateral clustering typical of mixed homopolymer brushes [61], or segment segregation seen in block copolymer brushes [45, 58], both of which can cause spatial chemical heterogeneities on the scale of 10 nm or more. Accordingly, if local surface-chemical homogeneity is needed from a surface chemistry gradient library, statistical copolymer gradients present an advantage.

Grafted homopolymer and copolymer gradient libraries have a tremendous potential for the high-throughput examination of both brush properties and applications involving grafted polymer layers. For example, NIST researchers Xu et al. [57, 58] used such libraries to examine the ability of grafted block copolymers to change their surface segment expression under different environments. This “switching” behavior can be harnessed to create “smart” coatings and surfaces that change their wetting, adhesion, and other properties in response to environmental triggers. The NIST study examined environmental response of the series of PnBMA-b-PDMAEMA block copolymer libraries shown in Fig. 11b. In this system, the PDMAEMA (top) block segments are preferentially solvated by water, while hexane is a preferential solvent for the PnBMA (bottom) blocks. Basically, the gradient experiment involved an assessment of the expression of PnBMA and PDMAEMA segments at the surface of the brush after the library was treated with water and then hexane. Water contact angle measurements along the library were used to estimate the degree of segment surface expression, based on the known equilibrium water contact angles for the pure polymer species (about 90° for PnBMA and approximately 65° for PDMAEMA). The results of these experiments for three libraries, each with a different PnBMA block length, can be seen in Fig. 12. In this plot, the brush is shown to “switch” its surface expression of segments between the block species when the measured contact angle changes due to water or hexane exposure. If the contact angle remains the same, it indicates that the segments were unable to significantly rearrange. The power of the gradient approach to this system is that it clearly outlines how molecular parameters govern the diblock switching behavior. In addition, it provides a view of narrow windows of optimal response that would be quite difficult to observe in single specimens. The library shows that longer PDMAEMA blocks suppress switching, while longer PnBMA blocks enhance the system’s ability to rearrange. In addition, the library illuminates the narrow ranges of molecular architecture that result in the maximum changes in segment expression at the surface. For example, for the data shown in red this optimal switching occurs in a window of top block thickness that is only 4 nm wide.

Grafted polymer libraries were also used by NIST researchers to achieve a variety of other measurements. For example, Mei and coworkers [59] leveraged their gradient in polymer grafting density to assess brush biocompatibility. In particular, they used this approach map the effect of poly(2-hydroxyethyl methacrylate) grafting density on the level of fibronectin adsorption and subsequent cell binding. The library enabled the team to determine rapidly the complex correlations between polymer grafting density, fibronectin coverage and cell adhesion, as well as the optimal surface conditions for cell proliferation. In another emerging example, Patton and coworkers [62] demonstrated how μ -SIP can be leveraged to measure rapidly and reliably copolymer reactivity ratios, which link the composition

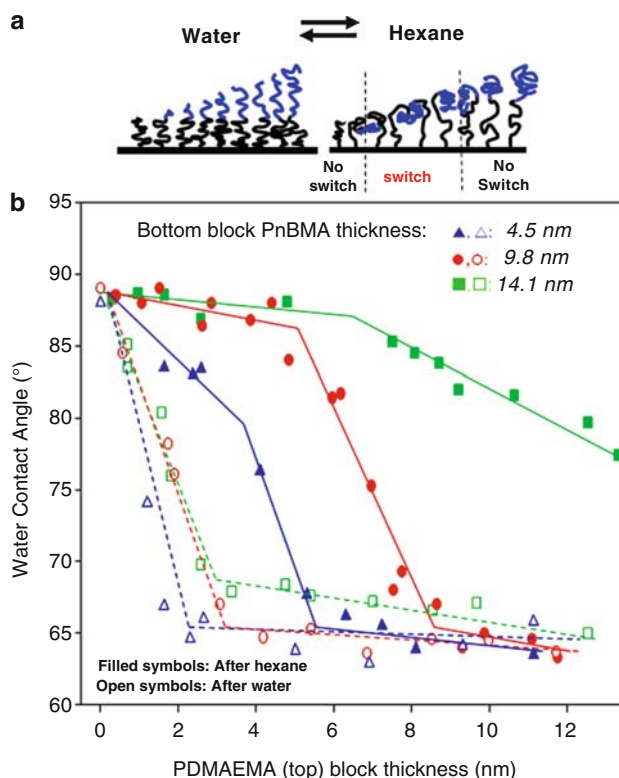


Fig. 12 Surface expression of block segments in block copolymer gradient libraries after treatment to two solvents. See text for details: **a** illustration of surface expression of PnBMA (*black*) and PDMAEMA (*blue*) block copolymer brush segments after water and hexane treatments; **b** water contact angle data from three PnBMA-*b*-PDMAEMA block copolymer gradient libraries after hexane (*filled symbols*) and water (*open symbols*) treatments. (Derived from [58] with permission)

of mixed monomer polymerization solutions to the composition of copolymer species. Knowledge of reactivity ratios is extremely important for synthesizing polymers with tailored composition and architecture, but they are difficult and time-consuming to measure. The researchers showed that by measuring the composition of the monomer solution in the microchannel (e.g., via a fiber optic Raman spectroscopy probe) and correlating it to the composition of the statistical copolymer brush created on the surface (measured by X-ray photoelectron spectroscopy, XPS), reactivity ratios could be determined. While the published study involved a series of discrete specimens, the extension of the measurement approach to gradient libraries is straightforward. This team is currently establishing protocols to reliably achieve this by combining Raman spectroscopy along a μ -SIP solution gradient and automated XPS data collected from a gradient statistical copolymer library of the type illustrated in Fig. 10b.

3.5 Polymer Blend Composition Gradients

In “hard” materials, such as metals or oxides, the creation of composition gradients is enabled by the excellent atomic-level mixing inherent to co-sputtering, co-evaporation and other co-deposition techniques [63]. The creation of composition spreads in polymers can be more difficult, since the size of macromolecules and the higher viscosity of their solutions can inhibit the proper mixing required for reliable libraries. At NIST, Meredith and coworkers addressed this challenge by combining the flow coating apparatus with an automated syringe-based deposition of blended polymer solutions [3]. A schematic of this approach can be seen in Fig. 13. To start, solutions of the polymers (A and B in the figure) to be blended are prepared using a common solvent. These solutions are fed, and then continuously mixed, in a common vessel (Fig. 13a). The solution feeds are ramped over time such that the mixed solution begin with 100% B solution and ends with 100% A solution. As the composition of the mixed solution changes, a narrow bore syringe is used to collect gradually an aliquot from the vessel, capturing a column of solution that has a gradient in its composition from top to bottom. The narrow bore of the syringe inhibits mixing long enough so that it can be deposited as a strip onto a flat substrate (Fig. 13b). Then the flow coater blade (moving at constant velocity) is used to spread the strip into a thin film with level thickness (Fig. 13c). When the solvent evaporates, the resulting rectangular film library has a gradient in polymer composition that ranges from nearly 100% A to nearly 100% B.

There are some limitations to this technique. First, proper mixing can only be achieved with dilute, low viscosity polymer solutions (perhaps a few percent polymer by mass), so the final films are at most a few hundred nanometers thick. This can be a problem if confinement will create undesired effects in the blend behavior.

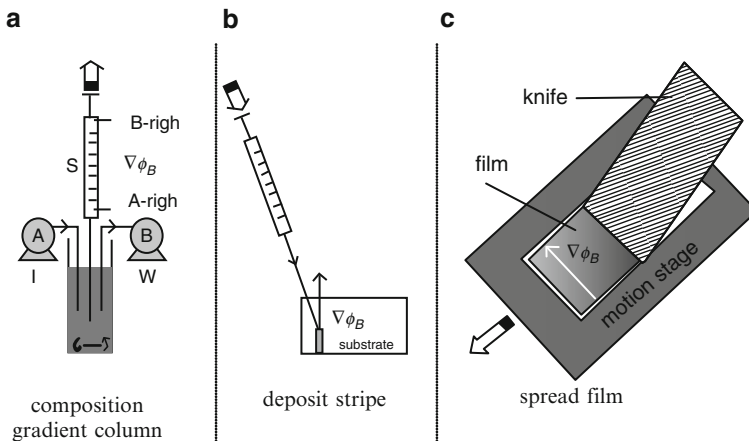


Fig. 13 Illustration of a method for producing polymer blend composition gradient libraries. A and B are the polymer solutions to be blended. ϕ_B is the relative volume concentration of the B polymer solution. See text for details. (Reproduced with permission from [3])

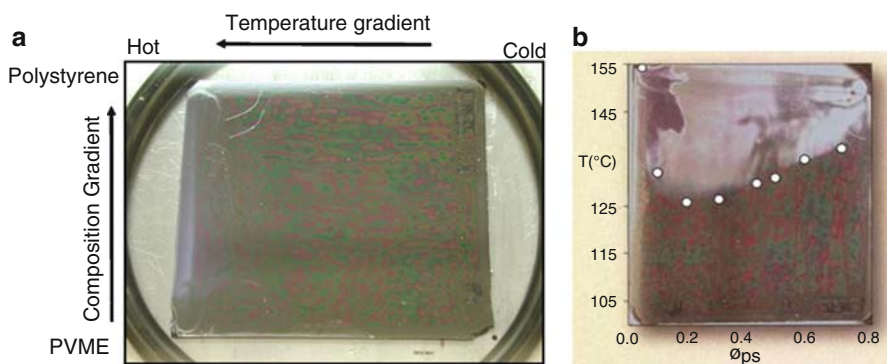


Fig. 14 Creation of a single specimen polymer blend phase diagram from orthogonal polymer composition and temperature gradients. The polymers are polystyrene and poly(vinyl methyl ether) (PVME): **a** composition library placed orthogonal to a temperature gradient; **b** completed gradient library polymer blend phase diagram. White points are data derived from traditional measurement for comparison. See text for details. (**b** reproduced with permission from [3])

In addition, the method only works for polymer pairs that can be blended in a common solvent. Nevertheless, this can be an extremely powerful method for assessing the behavior and performance of polymer blends. For example, Meredith et al. demonstrated the application of this approach to the high-throughput analysis of polymer blend phase behavior. Using polystyrene (PS) and poly(vinylmethylether) (PVME) as a test system, these authors created a single specimen polymer phase diagram by placing a PS-PVME gradient library on a gradient hot stage, as shown in Fig. 14. After annealing over the range of temperatures across the gradient hot stage, the library developed a hazy region, indicative of phase separated polymer domains. Where the polymer remained mixed, the film retained its smooth, as-cast appearance. As shown in Fig. 14b, these hazy and smooth regions delineate the miscibility gap of the PS-PVME blend system. The resulting polymer blend phase diagram library captures the entirety of this system's phase behavior in a single specimen.

Several research teams have employed this method for the high-throughput investigation of more complex polymer blend behavior and performance. For example, Karim and coworkers [64] used the method to screen the shifts in polymer miscibility induced by the addition of clay nanoparticles. In another study, a blend system slated for biomaterials applications was examined by Meredith et al. [65]. In this work, after the gradient phase diagram was created and cooled, cells were seeded across the library. A subsequent stain for cell viability indicated at which locations across the library cells adhered and propagated. Thus, in a single library experiment, the researchers could create a comprehensive map of which blend compositions and morphologies were biocompatible. More recently, Simon and coworkers [66] adapted this method to create microporous 3D gradient polymer blend specimens to investigate tissue scaffold materials. Instead of spreading a graded polymer concentration solution on a flat substrate, the researchers deposited it along a trough filled with salt crystals. Freeze-drying to remove the solvent and dissolution of the

salt resulted in a porous monolith (roughly 1 cm × 1 cm × 5 cm in dimension) that gradually changed in its composition from one end to the other. A first application of this technique resulted in the identification of the optimal level of iodinated polymer additive needed to create contrast in X-ray imaging measurements (e.g., X-ray tomography) of polymer tissue scaffolds [67]. In this study, the gradient polymer blend composition library was fabricated so that it gradually increased in the level of iodinated species along its length. A single X-ray radiography image of the entire library thus provided a comprehensive map of X-ray adsorption levels as a function of position. Using only two such libraries, they were able to determine the minimal levels of contrast agents required for four X-ray imaging processes. By traditional methods, similar optimization would have required preparation of nearly 100 specimens, followed by many hours of imaging measurements.

4 High-Throughput Materials Testing: Surfaces, Interfaces, and Thin Films

In order to tailor the function and properties of next-generation coatings and adhesives, industry researchers need to understand and control the complex interactions of material interfaces. However, the properties of interfaces are often difficult to measure, since they are complex in their structure and chemistry, and depend on the interplay between multiple variables. Consequently, high-throughput measurements of surfaces, interfaces, and thin films are essential for developing structure-property relationships of coatings and adhesives generated using combinatorial strategies such as those presented in the previous sections. The NIST program has focused on enabling measurements of intrinsic properties of polymer films such as the Young's modulus, an extensive property of a material, as well as extrinsic properties such as adhesion, which depends on a multitude of factors such as modulus, surface energy, and surface roughness. In designing these types of measurement platforms, we discovered that some approaches are amenable to performing highly-parallel measurements on combinatorial libraries; thus, we could provide rapid, multiple-point measurements of a particular response. However, other approaches, due the very nature of the measurement method itself, did not lend themselves to parallel measurements; thus, we incorporated high-throughput, single point measurements of combinatorial libraries into our experimental design. In the following sections, examples of each type of measurement workflow will be highlighted.

4.1 Thin Film Mechanical Properties

Nanotechnology promises to revolutionize a growing set of materials applications ranging from technology sectors such as semiconductor manufacturing, advanced sensors and coatings, to biomedical sectors such as drug delivery and implant

devices. However, the quest to engineer materials on the nanoscale (e.g., in the form of ultrathin films) is met with the daunting task of measuring the physical and mechanical properties of these systems. Given that the material properties of thin films can be drastically different from that of the bulk material, understanding the mechanical properties of nanofilms is especially critical not only for engineering robust fabrication techniques but also for defining application thresholds and operating windows. Maintaining or even improving device performance and reliability while concurrently shortening overall time-to-market is strongly dependent on the ability to rapidly and quantitatively measure the mechanical properties of thin films and coatings. At NIST, we developed several combinatorial and high-throughput measurement platforms that probe the mechanical properties of thin film libraries. In particular, we incorporated combinatorial libraries into an established methodology based on deformation of a thin film on a copper grid to investigate crazing and fracture in thin coatings. We also pioneered a new methodology based on surface wrinkling to rapidly measure the elastic modulus of thin films and coatings. These two measurement platforms underscore many of the challenges and opportunities presented by combinatorial and high-throughput experimental design.

4.1.1 Crazing in Thin Polymer Films

Upon application of strain, polymeric materials can undergo local deformation and yielding processes such as crazing, which leads to the formation of small fibrils and microvoids. These fibrils and microvoids effectively increase the fracture toughness of the material by absorbing energy prior to large-scale cracking in the material [68]. Since many applications of polymers employ thin coatings that are exposed to relatively large stress fields, it is imperative to understand crazing in thin film geometries. The copper grid technique [69] applies a uniaxial strain to a thin polymer film mounted onto a ductile copper grid (see Fig. 15). Due to plastic deformation of the copper, a portion of the applied strain is transferred to and remains in the

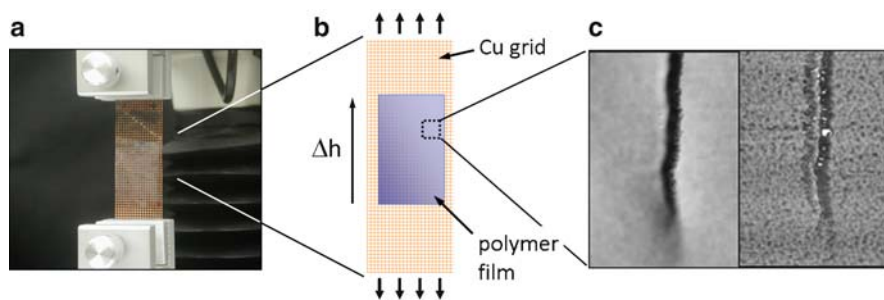


Fig. 15 **a** Digital image of a copper grid-supported thin polystyrene film clamped in a uniaxial tensile machine. **b** Schematic of a thickness gradient film mounted for conducting a copper grid strain test. **c** AFM images (height and phase) of a craze tip after deformation. (Derived from [70] with permission)

attached polymer film, even after the sample has been removed from the tensile testing instrument. This feature allows for the quantitative assessment of craze microstructure, craze distribution and film integrity. Observation of specimen deformation is achieved by monitoring the material suspended across the grid holes. The fracture processes within each grid space act independently and represent individual experiments. Accordingly, copper grid testing of gradient specimens enables parallel screening of craze behavior over the parameter space embodied by a combinatorial library. The ability to analyze rapidly multiple combinations of variables affecting crazing on a single sample eliminates potential variability and measurement error associated with sample preparation, processing and storage, while at the same time increasing measurement efficiency. Shallow thickness gradients allow comparatively uniform films to be presented across each grid square, thus yielding the equivalent of up to 30 or more different films that can be analyzed under identical conditions. The grid holes orthogonal to the thickness gradient can provide statistics of the crazing process, or a second gradient, such as film composition or crystallinity, can be incorporated into the film, thereby greatly increasing the parameter space studied. Using this technique, NIST researchers demonstrated that this method provides quantitative characterization of craze dimensions in glassy polymer films. Interestingly, those results indicated that craze widening and micro-necking mechanisms are quantitatively continuous in films with thickness greater than 50 nm [70].

4.1.2 Thin Film Modulus Measurements

While the copper grid test captures the crazing and fracture behavior of thin polymer films, it does not provide any measure of the fundamental mechanical properties of these materials (e.g., the elastic modulus). The most common method for probing the modulus of thin coatings and films is instrument indentation (nanoindentation or AFM), which has proven extremely valuable in the field of hard materials such as metallic and ceramic materials. Despite the success of instrumented indentation, there continues to be a number of technical issues impeding accurate indentation measurements on thin polymer films, the most notable being the so-called substrate effect which necessitates that the indentation depth be less than 10% of the total film thickness. Such shallow indentation depths become increasingly impractical or difficult as the film thickness approaches 100 nm or less. Furthermore, when studying polymer films, it is difficult to detect when the indenter establishes contact with the surface due to the extremely low loads encountered with softer materials (MPa to GPa).

To address this measurement need, NIST researchers developed a novel methodology based on surface wrinkling to assess the mechanical properties of thin polymer films [71,72]. Surface wrinkling occurs upon compression of a bilayer laminate comprised of a stiff, thin coating supported by a thick, soft substrate. In order to minimize the applied strain energy, the system undergoes a mechanical instability having a defined wavelength (λ), which can be related to the elastic modulus of the stiff coating by

$$\bar{E}_f = 3\bar{E}_s \left(\frac{\lambda}{2\pi h_f} \right)^3 \quad (1)$$

where h is the thickness, $\bar{E} = E/(1 - \nu^2)$ is the plane-strain modulus (E is the elastic modulus, ν is the Poisson's ratio, and the subscripts "f" and "s" denote the film and substrate, respectively). In nearly all studies to date, NIST researchers and others have employed crosslinked poly(dimethyl siloxane) (PDMS, $E \approx 2$ MPa) as the substrate. Because the substrate modulus (E_s) and film thickness (h_f) can both be independently measured by traditional techniques, the wavelength of the wrinkling provides a window for measuring of the modulus of the stiff, thin coating (E_f). The wavelength of the wrinkling instability can be measured rapidly by a number of techniques such as laser light diffraction, optical microscopy, or AFM. In the case of light diffraction, the sample can be rastered across the beam to map out the mechanical properties of the entire film, providing rapid analysis of, for example, a gradient library. Conversely, if the sample is uniform, a multitude of images can be acquired to improve the statistics of a single measurement.

Figure 16 demonstrates the range of moduli that can be assessed using the wrinkling metrology, as well as the precision of these measurements. Figure 16a shows moduli data collected along a thickness gradient library of polystyrene [PS], illustrating the ability of this technique to measure the modulus of glassy polymer films ($E \approx 1$ –5 GPa), as well as its use in a combinatorial workflow. In the example shown in Fig. 16a, the average value for the modulus was $3.4 \text{ GPa} \pm 0.1 \text{ GPa}$, in excellent agreement with reported bulk values for PS measured via conventional techniques such as tensile testing [73]. The surface wrinkling metrology can also measure soft materials, such as poly(styrene–isoprene–styrene) [P(S–I–S)] block copolymers, that display moduli in the MPa range (Fig. 16b). Our surface wrinkling metrology can easily discriminate materials having less than a 5% difference in moduli, which demonstrates the unique power of this metrology for thin polymer film research. This point is illustrated in Fig. 16c, where the modulus of ultrathin PS films is shown to decrease sharply when the film thickness decreases below $\approx 40 \text{ nm}$ [74].

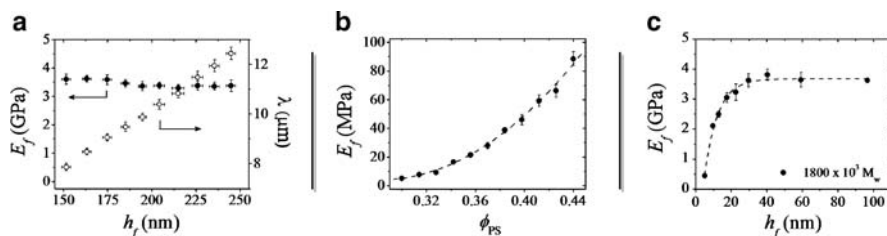


Fig. 16 Representative data from the surface wrinkling metrology, demonstrating the unprecedented range of moduli and the precision that the methodology unlocks: **a** modulus of a thickness gradient library of PS (reproduced with permission from [72]); **b** modulus as a function of composition for P(S–I–S) triblock copolymer blends; **c** modulus as a function of thickness for ultrathin PS films (reproduced with permission from [74]). The *lines* are meant to guide the eye and the *error bars* represent one standard deviation of the data, which is taken as the experimental uncertainty of the measurement

Our metrology has also been applied to particularly challenging systems, such as layer-by-layer assemblies [75–77], polymer brushes [78], and even single carbon nanotubes [79], with remarkable results.

The mechanics of surface wrinkling necessitate that there be a reasonable modulus difference between the film of interest and the soft substrate ($E_s \approx 2\text{MPa}$ for PDMS). In order to probe softer materials, the wrinkling metrology can be inverted, such that a sensor film of known modulus is adhered to a soft substrate of unknown modulus. Rearrangement of (1) leads to the following expression for the modulus of the soft, elastic substrate:

$$\bar{E}_s = \frac{\bar{E}_f}{3} \left(\frac{\lambda}{2\pi h_f} \right)^{-3} \quad (2)$$

Here, the unknown to be determined is the modulus of the soft elastic substrate, E_s . The thickness of the sensor film is chosen such that the wavelength of the wrinkling instability can again be measured by small angle light scattering (SALS), thus enabling high-throughput measurement of the substrate modulus. Experimental validation of this approach was conducted using a series of model crosslinked PDMS elastomers [80]. To extend the applicability of the buckling metrology as well as demonstrate its versatility, we investigated its use for determining the modulus of commonly used and commercially relevant poly(HEMA) hydrogels, which are widely used in the fields of contact lenses and biomaterials. Using this inverted geometry, we measured moduli of hydrated elastomers between $0.21\text{MPa} < E_s < 2.6\text{MPa}$, greatly extending the demonstrated range of moduli that this surface wrinkling metrology can probe. Substrates containing either discrete or continuous gradients in modulus (via gradients in composition or crosslink density, for example) can be easily integrated into this measurement workflow.

4.2 Adhesion Testing

The ability to control and tailor the adhesion at various interfaces plays a critical role in numerous technologies including electronic packaging, coatings and paints, biomedical implants, and pressure sensitive adhesives (PSAs). Previous research has shown that polymer interface formation and failure is dependent upon a range of material, processing and testing parameters. Current (traditional) approaches to the characterization of adhesion have focused on isolating a single adhesion-controlling parameter and correlating the changes in adhesion with corresponding changes in that single parameter. However, these types of approaches are time-consuming, discrete, and do not allow interplay between variables to be investigated. Indeed, one major challenge in this field is the efficient exploration of this large parameter space in order to develop an understanding of the fundamental driving forces for development of adhesive strength at polymer/polymer, polymer/metal, polymer/ceramic, and polymer/biomaterial interfaces. The ability to conduct highly

parallel tests and employ multivariant libraries is an essential step toward rapidly and efficiently identifying structure-property relationships critical for tuning adhesive performance [81, 82]. At NIST, we developed several combinatorial and high-throughput measurement platforms for probing both the fundamental origins of adhesion (e.g., interfacial interactions) as well as practical aspects of adhesion in soft materials (e.g., PSAs) as well as glassy materials and thermosets (e.g., epoxies).

4.2.1 Viscoelastic Materials: Peel Tests

The peel test is one of the most common techniques to assess the adhesive properties of PSAs. As the demand increases for combinatorial tools to test material performance rapidly, applying combinatorial and/or high-throughput approaches to the peel test could yield valuable insight into PSA structure-property relationships as well as open the door to a larger parameter space that can be rapidly and efficiently explored [83, 84]. However, there are considerable technical challenges presented by adapting conventional peel tests to include combinatorial or high-throughput concepts. To illustrate some of these challenges, we consider a simple example: measuring the adhesive strength of a commercial PSA tape adhered to a glass substrate possessing a surface energy gradient ($\Delta\gamma$) along the peel direction (see Fig. 17a). The peel force (F) is averaged across the peel width (b), thus severely limiting the ability to apply an orthogonal gradient in this geometry. However, by combining both a gradient that increases in surface energy ($+\Delta\gamma$) and one that decreases in surface energy ($-\Delta\gamma$) relative to the peel direction, we can probe the effect that the gradient itself has on the peeling process (e.g., crack acceleration or deceleration, stick-slip, etc). As shown in Fig. 17b, the resulting peel data correlate well with the changing surface energy of the substrate. While this example demonstrates

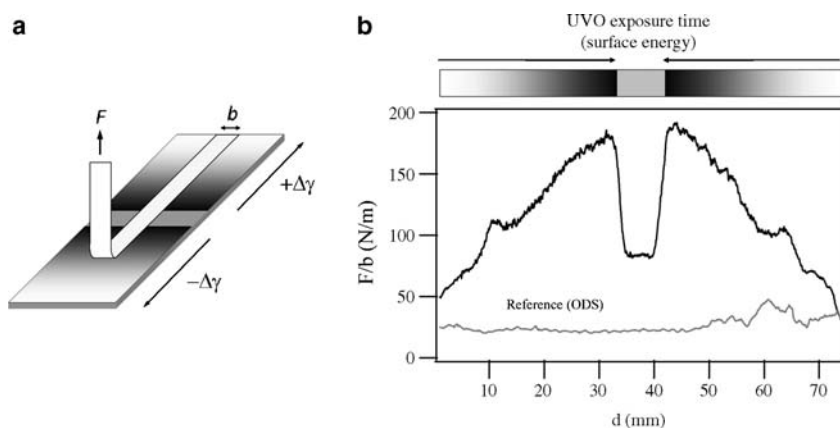


Fig. 17 **a** Schematic of peeling of an adhesive tape off a surface energy gradient. **b** Peel data (F/b) as a function of distance (d) along the surface energy gradient. As a reference, a traditional (non-gradient) peel test was also performed on the low surface energy substrate

the utility and value of combinatorial approaches as applied to peel tests, it also highlights a drawback: the lack of ample statistical information that is inherent in this type of measurement. For example, a conventional peel test conducted under constant conditions results in a fluctuating force to be averaged. Applying a continuous gradient of sample properties or test conditions in the peel direction implies that each data point (force) corresponds to a single point in parameter space, thus prohibiting the average force to be calculated for a given condition. To address this issue, we developed [83] a simple statistical treatment that allows a relationship between the uncertainty of the force and the domain size to be established. This statistical tool enables one to define the gradient step size (discrete gradients) or gradient steepness (continuous gradients) such that sound statistical information can be obtained and measurement uncertainties can be defined.

4.2.2 Viscoelastic Materials: Probe Tack Tests

Another common method for measuring adhesion strength in soft adhesives is the probe tack test, which involves bringing a rigid probe of known geometry into and out of contact with a flat adhesive layer while recording the applied displacement and resulting force throughout the cycle. In most cases, the probe geometry is either a cylindrical punch or a hemispherical lens. Since one needs to measure both force and displacement, it is difficult to design a parallel screening approach to this measurement platform. Therefore, the focus has been primarily on developing appropriate combinatorial libraries that span the parameter space of interest, while employing single point measurements of probe tack [85, 86]. At NIST we used this approach to examine the effect of temperature on the adhesive properties of model PSAs (see Fig. 18). In this study, a temperature gradient is established across a transparent sapphire window that is coated with a soft adhesive. The transparent substrate allowed us to image simultaneously the contact zone from below the sample, yielding valuable information about the failure mechanisms of the adhesive. Although tack tests were conducted in a serial manner across the temperature

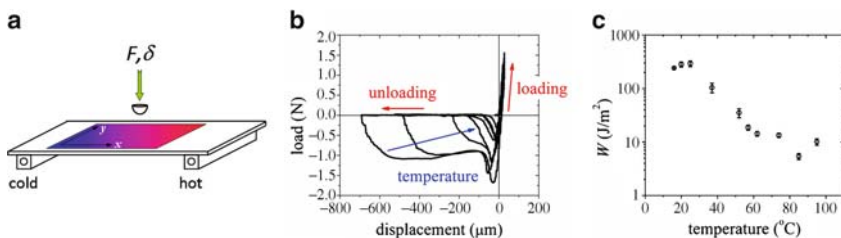


Fig. 18 **a** Schematic of probe tack measurements of a thin adhesive film along a temperature gradient. **b** Compilation of probe tack data during loading and unloading cycles for different temperatures. **c** Total adhesion energy, calculated from the area under the load-displacement curve shown in **b** divided by maximum contact area, as a function of temperature. The error bars represent one standard deviation of the data, which is taken as the experimental uncertainty of the measurement. (Reproduced with permission from [86])

gradient, our design yielded a dramatic decrease in the total measurement time to adequately survey the entire temperature range studied. For example, adhesion measurements at ten different temperatures by conventional tack tests would take 330 min [(30 min equilibration at each temperature + 3 min for tack test) \times 10 different temperatures], while adhesion measurements using the temperature gradient tack apparatus would only take 60 min [30 min equilibration on temperature gradient + (3 min for tack test \times 10 different temperatures)]. Thus, by incorporating a temperature gradient stage, we realized more than a fivefold increase in measurement throughput. We believe this new high-throughput technique has considerable analytical utility because several critical pieces of information can be acquired simultaneously and more efficiently, thus reducing experimental uncertainties and overall measurement time. In this initial study, we conducted only 1D in situ tack measurements, opting to use the second dimension to conduct multiple identical tests for statistical purposes, but more advanced applications are possible. For example, combinatorial aging tests and kinetic studies of epoxy curing can be examined using this instrument. By introducing another parameter such as aging or curing time, 2D libraries (e.g., time and temperature) can be easily generated and screened by probe-type tack measurements.

4.2.3 Glassy Materials: Edge-Delamination Tests

Combinatorial and high-throughput measurements of adhesion in rigid coatings and films demand quite different approaches than soft adhesives such as PSAs [81, 87, 88]. For example, contact methods such as the probe tack test are not suitable for measuring the interfacial strength of a coating adhered to a substrate. To this end, NIST researchers adapted the edge-delamination test [89] to evaluate the adhesion of combinatorial coating libraries to various substrates. In the edge-delamination test, thermal stress arising from cooling of a film/substrate system can propagate an initial crack along the film–substrate interface. Debonding occurs at a critical temperature (T_c) due to the stress concentration near the crack tip. The critical stress (σ_c) necessary to debond the film can be calculated using (3):

$$\sigma_c = \frac{E_f}{1 - \nu} (\alpha_s - \alpha_f) (T_c - T_{\text{ref}}) \quad (3)$$

where E is the elastic modulus, α is the coefficient of thermal expansion, and T_{ref} is a reference temperature where the film is assumed to be in a stress-free state and is usually chose to be the T_g of the film. The subscripts “f” and “s” denote the film and substrate, respectively. If the failure is assumed to take place in the film very near the interface (cohesive failure), the thermal stress at the critical temperature for debonding can be related to the fracture energy (K_{IC}) of the film:

$$K_{\text{IC}} = \sigma_0 \sqrt{\frac{h_f}{2}} \quad (4)$$

Thus, K_{IC} can be used as an accurate descriptor of the interfacial strength in a film/substrate system.

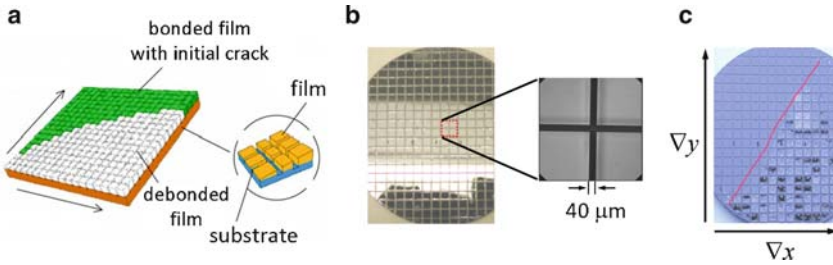


Fig. 19 **a** Schematic of the combinatorial edge-delamination test for probing interfacial adhesion strength. The gradient specimen is diced in order to mechanically isolate individual cells on the array as well as to provide an initial interfacial crack. **b** An optical micrograph of an individual element of the array illustrating the width and sharpness of the diced area. **c** Image of a gradient specimen after failure showing a distinct transition from bonded to debonded areas of the specimen. (Reproduced with permission from [91])

In order to adapt the edge-delamination test to combinatorial workflows, we first developed the framework of the metrology; this included theory, experimental design, stress analysis and simulation of the approach [90]. We could then employ combinatorial libraries that incorporate one or more adhesion-controlling parameters into the edge-delamination experimental design. For example, a film is coated onto a rigid substrate in such a way that the film has a gradient (e.g., thickness, surface energy, composition) in one direction, which is then subdivided into an array of separate edge-delamination samples, as depicted in Fig. 19a. This dicing process serves to generate a pre-crack at the film/substrate interface as well as to isolate mechanically each cell of the array from neighboring cells. A second orthogonal gradient could also be incorporated into the experimental design. The specimen is then slowly cooled and debonding events are observed for those sample cells having stresses greater than a critical value. These stresses depend on the combination of local temperature and film thickness. A map of failures can be constructed as a function of each unique combination of variable one and variable two (Fig. 19c). Subsequently, the interfacial strength between the film coating and the substrate can be deduced from the failure map using (4). We have demonstrated this methodology by probing the adhesion of thin PMMA films to a silicon substrate possessing a gradient in surface energy [91]. In that particular study, an epoxy stress-generating layer was coated directly on the PMMA films; an orthogonal thickness gradient of epoxy was applied to generate a gradient in the stress profile. We have also employed compositional gradients in epoxy films [92], as well as gradients in temperature (both curing temperature and quench temperature).

4.2.4 Elastic Materials: JKR Adhesion Tests

Oftentimes, in order to understand adhesion at the macroscale, we need to understand first the fundamental molecular interactions at interfaces. With this in mind,

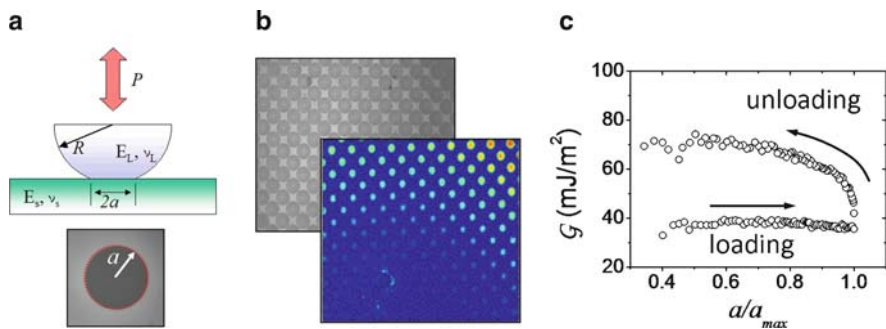


Fig. 20 **a** Test geometry for a single lens JKR test. The applied load (P), displacement (δ), and contact radius (a) are measured during a complete loading/unloading cycle. **b** Multilens array used for combinatorial adhesion measurements across a sample library, which can be combined with automated image analysis of the contact area across multiple lenses of the array to yield high-throughput measurements of adhesion across combinatorial libraries. **c** Representative data for \mathcal{G} for both loading and unloading segments of PDMS/PDMS contact. (**b** reproduced with permission from [95])

we developed a measurement platform to study quantitatively adhesion using the Johnson, Kendall and Roberts (JKR) model [93]. In this test, a hemispherical lens of one material is brought into and out of contact with a complementary substrate while measuring the applied load, displacement, and contact area between the lens and substrate (see Fig. 20a). The energy release rate (\mathcal{G}) represents the amount of energy required to change the contact area a unit amount, or more simply the additional energy required to drive the separation between the two surfaces, and is given by

$$\mathcal{G} = \frac{(P' - P)^2}{8\pi E^* a^3} \quad (5)$$

where $P' = \frac{4E^* a^3}{3R}$ is the Hertzian contact load (no adhesion), P is the applied load, E^* is the system modulus, and a is the contact radius. For a JKR test, the energy required to increase surface area during the loading curve is bounded by the thermodynamic work of adhesion (W), while the unloading segment provides a measure of the adhesion hysteresis (\mathcal{G}_{HYS}), which reflects specific adhesion interactions that develop while the lens is in contact with the substrate.

To facilitate high-throughput measurements on combinatorial libraries, we developed means to introduce a planar array of hemispherical lenses (see Fig. 20b) into contact with a substrate possessing a gradient in material properties or environmental parameters along one or both axes of the array [94, 95]. Conversely, the hemispherical lens array could embody one of the property gradients, such as a gradient in surface energy, or the lens array itself could be comprised of a material gradient, such as composition of the lenses within in the array. If two orthogonal gradients are placed on the array, then each lens contact point yields a measurement of adhesion for a unique combination of parameters. The challenge of using

a multilens array lies in the inability to measure load on each individual lens of the array. In this case, the displacement (δ) of the lens array (not the load (P), as in (5)) is used to calculate \mathcal{G} :

$$\mathcal{G} = \frac{E^* (\delta' - \delta)^2}{2\pi a} \quad (6)$$

where $\delta' = \frac{a^2}{R}$ is the Hertzian contact displacement.

We have employed microlens arrays that contain 100–1,600 individual lenses per cm^2 , depending on the sample size and steepness of the gradient under study. We have analyzed the effect of surface energy, crosslink density, and contact time using our multilens measurement approach. By integrating a temperature gradient into the instrument design, we can also measure temperature-dependent adhesive properties as a function of multiple variables. For example, in one study we measured the self-adhesion and fracture of polystyrene thin films using orthogonal gradients in temperature and film thickness [94]. This methodology is a powerful tool for investigating the effects of multivariable environments (e.g., surface energy, surface roughness, composition, and processing) on polymer adhesion. We are currently pursuing methods for functionalizing the PDMS lens array with different chemistries in a graded manner, such as layer-by-layer deposition of polyelectrolytes [96] and growth of polymer brushes [78], in ways that express the chemical diversity inherent in many interfaces.

5 High-Throughput Materials Synthesis and Solution Characterization: Microscale Approaches to Polymer Library Fabrication in Fluids

One of the major advantages of the techniques described above is the ability to measure materials properties with significantly reduced quantities of sample. There are few robust synthetic techniques, however, that can produce only the quantities of polymer necessary for these types of measurements. The development of microfluidic devices presented an appealing technology for adaptation to addressing this problem by producing devices that could carry out polymer synthesis in microliter volumes with cheap and flexible reactors directly interfaced with high-throughput measurement methods.

Additional potential advantages associated with performing chemical reactions in the confined space of a microfluidic channel include improved heat transfer, uniform mixing profiles, faster variable changes and improved safety [97]. Combined with a high-throughput characterization strategy this extends the versatility of a microfluidic R&D platform to studying routes for improving control of molar mass, polydispersity, architecture and composition. Previous studies demonstrate that improved control of polymer products was obtained when reactions were carried out in a microfluidic or microreactor environment [98].

The NIST program had a two-pronged approach: (1) use microfluidic devices to manipulate the stoichiometry and other conditions of reactions to produce continuous gradients in polymer chain structures, and (2) exploit the small volumes used in microfluidic channels to carry out measurements on polymer solutions that traditionally require significantly larger volumes or longer times to measure. Examples that will be presented in this section include the preparation of continuous gradients of molecular weight using ATRP, dynamic light scattering (DLS) on a chip and high-throughput interfacial tension (IFT) measurements.

5.1 Controlled Polymer Synthesis in Microchannels

With the development of controlled radical polymerization, synthetic polymer chemists dramatically expanded the range of materials that could be controlled on the molecular scale. Controlled and high-throughput techniques are essential to the systematic survey of this vast parameter space. NIST chose to pursue the use of a technique with flexibility, ease of use, and sample volumes similar to those used in the other library design and measurement methods described above. Channels fabricated in both polymer/glass (Fig. 21a) [99, 100] and metal devices [101] were used depending on the conditions necessary for the reactions. Earlier polymeric devices were replaced by metallic devices when higher temperatures and longer reaction times were required.

The first reactions were carried out at room temperature in devices fabricated from a thiolene resin cured between two glass slides. 2-Hydroxypropyl methacrylate (HPMA) was polymerized by ATRP, and reaction kinetics similar to those obtained in a traditional batch reaction were obtained by adjusting the total flow rate of the fluid through the channel and treating the residence time in the channel as the reaction time (Fig. 21b,c) [102].

The correlation of residence time to reaction time is critical in the ability to treat the volume of the channel as a continuous gradient in molecular mass. ATRP is particularly well-suited to this type of device because the reaction can be initiated at a fixed mixing element at the head of the channel where a catalyst and initiator can be brought together. By replacing a small molecule initiator with a polymer chain capable of being reinitiated, copolymers could be prepared. This was done in the thiolene/glass devices with a poly(*n*-butyl methacrylate) block [103].

In order to access a wider variety of monomers, higher temperatures were necessary. Using an aluminum channel capped on one wall with a Kapton film, styrene, as well as several acrylates and methacrylates, were polymerized. Furthermore, block copolymers were also prepared from these more widely used polymers, and the devices were integrated with characterization techniques as described below [104]. Similar devices have been used to carry out anionic polymerizations as well [105].

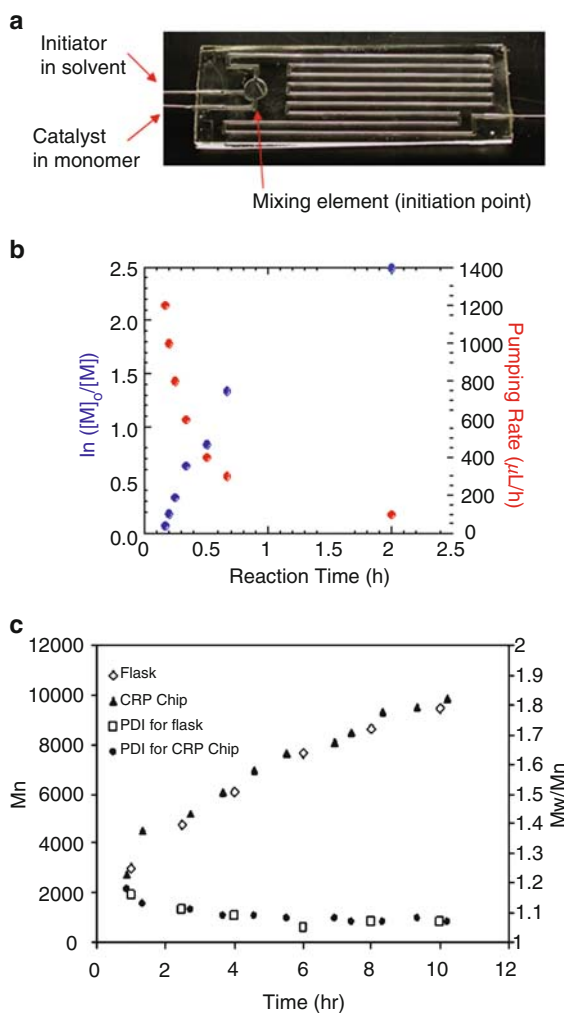


Fig. 21 Representative microfluidic device and resulting data from ATRP on a chip: **a** image of a microfluidic device (dimensions 25 mm × 75 mm) fabricated from UV curable thiolene resin between two glass slides; **b** reaction data for ATRP of HPMA synthesized on a chip showing the correlation of flow rate (or residence time) to reaction time and resulting conversion of monomer (M) to polymer ($\ln([M]_0/[M])$); **c** comparison of number average molecular mass (M_n) and polydispersity for *n*-butyl acrylate prepared in a traditional round bottom flask ('Flask') and on a chip ('CRP Chip'). (Reproduced with permission from [102])

5.2 Characterization of Interfacially-Active Polymers in Microchannels

In order to obtain the advantage of other high-throughput and combinatorial techniques in microfluidic reactors, it is critical that other processing and measurement

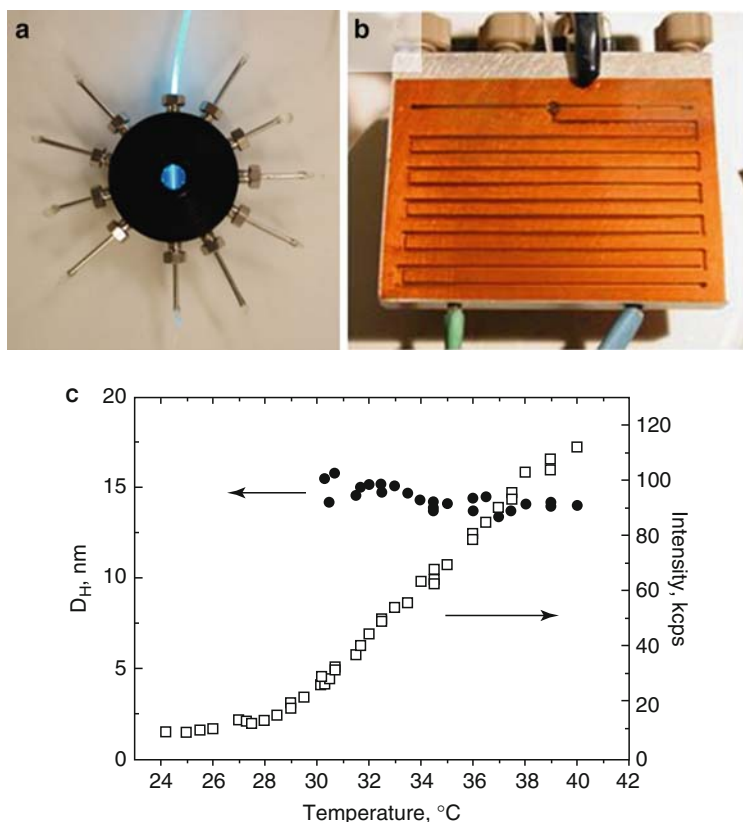


Fig. 22 Images and data representing development and application of DLS on a chip: **a** one iteration in the design of a microfluidic DLS fabricated from aluminum with the surface anodized black to reduce surface reflections; **b** image of a microfluidic chip that integrates polymer synthesis with DLS. The machined channels have been covered by a Kapton sheet fixed with adhesive; **c** data for temperature depended micelle formation of polyethylene oxide–polypropylene oxide–polyethylene oxide triblock copolymer (Pluronic P85) at 2% by volume in water. (Derived from [106] with permission)

tools be integrated into the same platform. The NIST team designed a dynamic light scattering (DLS) instrument on a chip by anodizing the inner walls of an aluminum channel to minimize reflections and plumbing the channel with fiber optics which both deliver an incident beam and detect off-axis scattering (Fig. 22a). After several iterations of design [106], the DLS was applied to detect the formation of micelles in block copolymers as a function of cosolvent fraction (polystyrene/polyisoprene diblock copolymers in hexanes/toluene) or temperature (polyethylene oxide/polypropylene oxide triblock copolymers in water; Fig. 22c).

This new DLS tool was integrated into the microreactors by placing it at the end of a chip that synthesized amphiphilic block copolymers from methyl methacrylate and either lauryl methacrylate or octadecyl methacrylate (Fig. 22b). The reaction

mixture was then diluted with a selective solvent while still on the device, which both terminated the polymerization and induced micelle or other structure formation in the fluid. The structured samples then flowed through the DLS chamber for characterization of size [101]. The total sample volume in the DLS measurement chamber was only 4 μL , and the device enabled comparatively simple alignment procedures while reducing multiple scattering.

The integrated DLS device provides an example of a measurement tool tailored to nano-scale structure determination in fluids, e.g., polymers induced to form specific assemblies in selective solvents. There is, however, a critical need to understand the behavior of polymers and other interfacial modifiers at the interface of immiscible fluids, such as surfactants in oil-water mixtures. Typical measurement methods used to determine the interfacial tension in such mixtures tend to be time-consuming and had been described as a major barrier to systematic surveys of variable space in libraries of interfacial modifiers. Critical information relating to the behavior of such mixtures, for example, in the effective removal of soil from clothing, would be available simply by measuring interfacial tension (IFT) for immiscible solutions with different droplet sizes, a variable not accessible by drop-volume or pendant drop techniques [107].

Through many iterations of design, NIST scientists developed a microfluidic chip that addressed this challenge, by forming droplets of immiscible fluids in a continuous flow stream, while systematically varying conditions that would influence the interfacial tension between the two fluids. The device consisted of three basic elements: drop formation, mixing and drop adsorption, and drop deformation, followed by detection of the drop relaxation using a charge-coupled device (CCD) camera. A variety of mixtures were characterized with these techniques, including the siloxane interface with water, air, ethylene glycol and glycerol, with and without added surfactants (Fig. 23a) [108].

Challenges associated with the proper design of the instrument on a chip included consideration and elimination of confinement effects, depletion issues when the surfactant concentration was determined by the size of the droplet (i.e., the droplet phase contained the surfactant additive) and full automation of fluid controls, image capture and data analysis. Ultimately, however, the device was demonstrated to measure both equilibrium and dynamic IFT in a fraction of the time necessary by conventional techniques and at a length-scale of greater relevance to the applications of interest. The rapid scanning of composition variation was demonstrated by measuring the IFT of water/ethylene glycol mixtures in polydimethylsiloxane oil (Fig. 23b) [109].

6 Conclusions

We provided an overview of combinatorial and high-throughput methods research at NIST, with a focus on tools and application examples that are useful for the examination of polymer surfaces, interfaces and thin films. An examination of this body

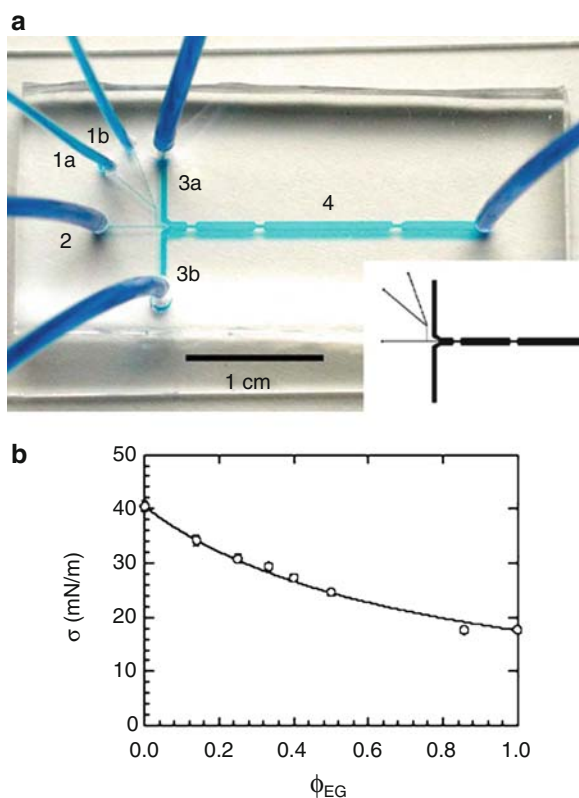


Fig. 23 **a** Image of a microfluidic chip used for IFT measurements filled with liquid dye to illuminate channels. To perform the measurement, drops are injected (fluid 1a and b) are injected into an immiscible stream (2). Additional immiscible matrix is added (3a and 3b) conveying the drops into channel 4 for analysis and measurement. Constrictions in channel 4 accelerate/stretch the drops. Multiple constrictions enable measurement at different interface age. The channel geometry is shown schematically in the *inset* (from [108]). **b** Interfacial tension (σ) of water/ethylene glycol mixtures (binary drops) in PDMS oil, as a function of composition (ϕ). (Reproduced with permission from [109])

of work illustrates two key points that are worth discussing in conclusion. First, it is clear that gradient and microfluidic methods are powerful tools for polymer research, and this is not only because these techniques can be more rapid (although, this is one great advantage). A more important aspect, especially for emerging polymer technologies, is that these techniques allow scientists and engineers to approach complex materials systems in ways that are impossible via traditional techniques. As illustrated in many of the examples discussed above, a library approach enables the researcher to view, often in a single specimen, an entire space of structures, behaviors and their response to influencing variables. These “big picture” snapshots can be invaluable in initiating and building a comprehensive understanding

of complex systems and the factors that govern them. In addition, gradient libraries enable the researcher to “zoom in” on specific parameter subsets to achieve more detailed analyses; this unique capability facilitates a more rigorous examination of the structure-processing-performance interrelationships that are key to materials science and engineering.

The second point is that, quite often, library approaches can provide significant advantages even if they are not integrated into extensive workflow infrastructures that are often associated with combinatorial methods. Indeed, gradient libraries and microfluidic library synthesis can provide extensive benefits both in their own right and in combination with modest automated analysis. The “self-reporting” aspect of gradient libraries is one example of this, as is the ability of continuous microreactors to create systematically changing families of polymer specimens while using minuscule amounts of reactant. Moreover, by pairing libraries with high-throughput measurement platforms researchers have access to an unparalleled, and rapid, ability to determine the factors that govern and optimize materials performance. Examples of this can be seen in our discussion of high-throughput adhesion and mechanical properties tests, which are fueled by appropriately fabricated library specimens. In addition, as we discussed, microfluidic technologies are quite powerful in this respect, since they can integrate library fabrication and high-throughput analysis of fluid specimens on a single device.

In each of these “take home” messages, the benefits of combinatorial and high-throughput approaches are gained by thinking beyond the single sample paradigm, by being aware of the opportunities afforded by developing and exploiting these tools, and by applying them with the wisdom that has always characterized successful polymers science.

References

1. Webster DC (2005) Radical change in research and development: the shift from conventional methods to high-throughput methods. *JCT Coat Technol* 2:24–29
2. Hanak JJ (1970) Multiple-sample-concept in materials research – synthesis, compositional analysis and testing of entire multicomponent systems. *J Mater Sci* 5:964
3. Meredith JC, Karim A, Amis EJ (2000) High-throughput measurement of polymer blend phase behavior. *Macromolecules* 33:5760–5762
4. Meredith JC, Karim A, Amis EJ (2002) Combinatorial methods for investigations in polymer materials science. *MRS Bull* 27:330–335
5. Stafford CM, Roskov KE, Epps TH, Fasolka MJ (2006) Generating thickness gradients of thin polymer films via flow coating. *Rev Sci Instrum* 77:023908
6. Zhang X, Berry BC, Yager KG, Kim S, Jones RL, Satija S, Pickel DL, Douglas JF, Karim A (2008) Surface morphology diagram for cylinder-forming block copolymer thin films. *ACS Nano* 2:2331–2341
7. de Gans BJ, Wijnans S, Woutes D, Schubert US (2005) Sector spin coating for fast preparation of polymer libraries. *J Comb Chem* 7:952–957
8. Cull TR, Goulding MJ, Bradley M (2007) Liquid crystal libraries-ink-jet formulation and high-throughput analysis. *Adv Mater* 19:2355–2359
9. Meier MAR, Schubert US (2005) Integration of MALDI-TOFMS as high-throughput screening tool into the workflow of combinatorial polymer research. *Rev Sci Instrum* 76:062211

10. Yoshioka Y, Calvert PD, Jabbour GE (2005) Simple modification of sheet resistivity of conducting polymeric anodes via combinatorial ink-jet printing techniques. *Macromol Rapid Commun* 26:238–246
11. de Gans BJ, Kazancioglu E, Meyer W, Schubert US (2004) Ink-jet printing polymers and polymer libraries using micropipettes. *Macromol Rapid Commun* 25:292–296
12. Koner L, Kofler W (1949) A heating bed for rapid determination of the melting point. *Mikrochem Mikrohchim Acta* 34:374–381
13. Sehgal A, Karim A, Stafford CF, Fasolka MJ (2003) Techniques for combinatorial and high-throughput microscopy: part 1: gradient specimen fabrication for polymer thin films research. *Micros Today* 11:26–29
14. Beers KL, Douglas JF, Amis EJ, Karim A (2003) Combinatorial measurements of crystallization growth rate and morphology in thin films of isotactic polystyrene. *Langmuir* 19:3935–3940
15. Lucas LA, DeLongchamp DM, Vogel BM, Lin EK, Fasolka MJ, Fischer DA, McCulloch I, Heeney M, Jabbour GE (2007) Combinatorial screening of the effect of temperature on the microstructure and mobility of a high performance polythiophene semiconductor. *Appl Phys Lett* 90:012112
16. Eidelman N, Raghavan D, Forster AM, Amis EJ, Karim A (2004) Combinatorial approach to characterizing epoxy curing. *Macromol Rapid Commun* 25:259–263
17. Roberson SV, Faheya AJ, Sehgal A, Karim A (2002) Multifunctional ToF-SIMS: combinatorial mapping of gradient energy substrates. *Appl Surf Sci* 200:150–164
18. Smith AP, Sehgal A, Douglas JF, Karim A, Amis EJ (2003) Combinatorial mapping of surface energy effects on diblock copolymer thin film ordering. *Macromol Rapid Commun* 24:131–135
19. Berry BC, Stafford CM, Pandya M, Lucas LA, Karim A, Fasolka MJ (2007) Versatile platform for creating gradient combinatorial libraries via modulated light exposure. *Rev Sci Instrum* 78:072202
20. Elwing H, Welin S, Askendal A, Nilsson U, Lundström I (1987) A wettability gradient method for studies of macromolecular interactions at the liquid/solid interface. *J Colloid Interface Sci* 119:203–210
21. Chaudhury MK, Whitesides GM (1992) How to make water run uphill. *Science* 256:1539–1541
22. Genzer J (2005) Templating surfaces with gradient assemblies. *J Adhes* 81:417–435
23. Zhao H, Beysens D (1995) From droplet growth to film growth on a heterogeneous surface – condensation associated with a wettability gradient. *Langmuir* 11:627–634
24. Liedberg B, Tengvall P (1995) Molecular gradients of omega-substituted alkanethiols on gold – preparation and characterization. *Langmuir* 11:3821–3827
25. Liedberg B, Wirde M, Tao YT, Tengvall P, Gelius U (1997) Molecular gradients of omega-substituted alkanethiols on gold studied by X-ray photoelectron spectroscopy. *Langmuir* 13:5329–5334
26. Morgenthaler S, Lee S, Zurcher S, Spencer ND (2003) A simple, reproducible approach to the preparation of surface-chemical gradients. *Langmuir* 19:10459–10462
27. Morgenthaler SM, Lee S, Spencer ND (2006) Submicrometer structure of surface-chemical gradients prepared by a two-step immersion method. *Langmuir* 22:2706–2711
28. Ashley KM, Raghavan D, Douglas JF, Karim A (2005) Wetting-dewetting transition line in thin polymer films. *Langmuir* 21:9518–9523
29. Fasolka MJ, Mayes AM (2001) Block copolymer thin films: physics and applications. *Annu Rev Mater Res* 31:323–355
30. Smith AP, Douglas JF, Meredith JC, Amis EJ, Karim A (2001) Combinatorial study of surface pattern formation in thin block copolymer films. *Phys Rev Lett* 87:015503
31. Ludwigs S, Schmidt K, Stafford CM, Amis EJ, Fasolka MJ, Karim A, Magerle R, Krausch G (2005) Combinatorial mapping of the phase behavior of ABC triblock terpolymers in thin films: Experiments. *Macromolecules* 38:1850–1858

32. Epps TH, Delongchamp DM, Fasolka MJ, Fischer DA, Jablonski EL (2007) Substrate surface energy dependent morphology and dewetting in an ABC triblock copolymer film. *Langmuir* 23:3355–3362
33. Roskov KE, Epps TH, Berry BC, Hudson SD, Tureau MS, Fasolka MJ (2008) Preparation of combinatorial arrays of polymer thin films for transmission electron microscopy analysis. *J Comb Chem* 10:966–973
34. Julthongpiput D, Fasolka MJ, Zhang WH, Nguyen T, Amis EJ (2005) Gradient chemical micropatterns: a reference substrate for surface nanometrology. *Nano Lett* 5:1535–1540
35. Julthongpiput D, Zhang W, Douglas JF, Karim A, Fasolka MJ (2007) Pattern-directed to isotropic dewetting transition in polymer films on micropatterned surfaces with differential surface energy contrast. *Soft Matter* 3:613–618
36. Gallant ND, Lavery KA, Amis EJ, Becker ML (2007) Universal chemistry for “Click” chemistry biofunctionalization. *Adv Mater* 19:072207
37. Kolb HC, Finn MG, Sharpless BK (2001) Click chemistry: diverse chemical function from a few good reactions. *Angew Chem Int Ed* 40:2004–2021
38. Lin-Gibson S, Landis FA, Drzal PL (2006) Combinatorial investigation of the structure-properties characterization of photopolymerized dimethacrylate networks. *Biomaterials* 27:1711–1717
39. Lin NJ, Drzal PL, Lin-Gibson S (2007) Two-dimensional gradient platforms for rapid assessment of dental polymers: a chemical, mechanical and biological evaluation. *Dent Mater* 23:1211–1220
40. Johnson PM, Stansbury JW, Bowman CN (2007) Photopolymer kinetics using light intensity gradients in high-throughput conversion analysis. *Polymer* 48:6319–6324
41. Johnson PM, Stansbury JW, Bowman CN (2008) High-throughput kinetic analysis of acrylate and thiol-ene photopolymerization using temperature and exposure time gradients. *J Polym Sci Part A Polym Chem* 46:1502–1509
42. Johnson PM, Stansbury JW, Bowman CN (2008) Kinetic modeling of a comonomer photopolymerization system using high-throughput conversion data. *Macromolecules* 41:230–237
43. Matyjaszewski K, Miller PJ, Shukla N, Immraporn B, Gelman A, Luokala BB, Siclován TM, Kickelbick G, Vallant T, Hoffmann H, Pakula T (1999) Polymers at interfaces: using atom transfer radical polymerization in the controlled growth of homopolymers and block copolymers from silicon surfaces in the absence of untethered sacrificial initiator *Macromolecules* 32:8716–8724
44. Husseman M, Malmstrom EE, McNamara M, Mate M, Mecerreyes D, Benoit DG, Hedrick JL, Minsky P, Huang E, Russell TP, Hawker CJ (1999) Controlled synthesis of polymer brushes by “Living” free radical polymerization techniques. *Macromolecules* 32:1424–1431
45. Bhat RR, Tomlinson MR, Genzer J (2005) Orthogonal surface-grafted polymer gradients: a versatile combinatorial platform. *J Polym Sci Part B Polym Phys* 43:3384–3394
46. Genzer J, Bhat RR (2008) Surface-bound soft matter gradients. *Langmuir* 24(6):2294–2317
47. Wu T, Efimenko K, Genzer J (2002) Combinatorial study of the mushroom-to-brush crossover in surface anchored polyacrylamide. *J Am Chem Soc* 124:9394–9395
48. Wu T, Efimenko K, Vlcek P, Subr V, Genzer J (2003) Formation and properties of anchored polymers with a gradual variation of grafting densities on flat substrates. *Macromolecules* 36:2448–2453
49. Zhao B, Brittain WJ (2000) Polymer brushes: surface-immobilized macromolecules. *Prog Polym Sci* 25:677–710
50. Patten TE, Matyjaszewski K (1998) Atom transfer radical polymerization and the synthesis of polymeric materials. *Adv Mater* 10:901
51. Mendes PM (2008) Stimuli-responsive surfaces for bio-applications. *Chem Soc Rev* 37:2512–2529
52. La WH, Wang RM, He YF, Zhang HF (2008) Preparation and application of smart coatings. *Prog Polym Chem* 20:351–361
53. Patten TE, Xia JH, Abernathy T, Matyjaszewski K (1996) Polymers with very low polydispersities from atom transfer radical polymerization. *Science* 272:866–868

54. Prucker O, Ruhe J (1998) Synthesis of poly(styrene) monolayers attached to high surface area silica gels through self-assembled monolayers of azo initiators. *Macromolecules* 31:592–601
55. Prucker O, Ruhe J (1998) Polymer layers through self-assembled monolayers of initiators. *Langmuir* 14:6893–6898
56. Xu C, Wu T, Drain CM, Batteas JD, Beers KL (2005) Microchannel confined surface-initiated polymerization. *Macromolecules* 38:6
57. Xu C, Wu T, Batteas JD, Drain CM, Beers KL, Faselka MJ (2006) Surface-grafted block copolymer gradients: effect of block length on solvent response. *Appl Surf Sci* 252:2529–2534
58. Xu C, Wu T, Drain CM, Batteas JD, Faselka MJ, Beers KL (2006) Effect of block length on solvent response of block copolymer brushes: combinatorial study with block copolymer brush gradients. *Macromolecules* 39:3359–3364
59. Mei Y, Wu T, Xu C, Langenbach KJ, Elliott JT, Vogt BD, Beers KL, Amis EJ, Washburn NR (2005) Tuning cell adhesion on gradient poly(2-hydroxyethyl methacrylate)-grafted surfaces. *Langmuir* 21:12309–12314
60. Xu C, Barnes SE, Wu T, Fischer DA, DeLongchamp DM, Batteas JD, Beers KL (2006) Solution and surface gradients via microfluidic confinement: fabrication of a statistical copolymer brush composition gradient. *Adv Mater* 18:1427
61. Zhao B (2004) A combinatorial approach to study solvent-induced self-assembly of mixed poly(methyl methacrylate)/polystyrene brushes on planar silica substrates: effect of relative grafting density. *Langmuir* 20:11748–11755
62. Patton DL, Page KA, Xu C, Genson KL, Faselka MJ, Beers KL (2007) Measurement of reactivity ratios in surface-initiated radical copolymerization. *Macromolecules* 40:6017–6020
63. Zhao JC (2006) Combinatorial approaches as effective tools in the study of phase diagrams and composition-structure-property relationships. *Prog Mater Sci* 51:557–631
64. Karim A, Yurekli K, Meredith C, Amis EJ, Krishnamoorti R (2002) Combinatorial methods for polymer materials science: phase behavior of nanocomposite blend films. *Polym Eng Sci* 42:1836–1840
65. Meredith JC, Sormana JL, Keselowsky BG, Garcia AJ, Tona A, Karim A, Amis EJ (2003) Combinatorial characterization of cell interactions with polymer surfaces. *J Biomed Mater Res Part A* 66A:483–490
66. Simon CG Jr, Stephens JS, Dorsey SM, Becker ML (2007) Fabrication of combinatorial polymer scaffold libraries. *Rev Sci Instrum* 78:0722071
67. Yang Y, Dorsey SM, Becker ML, Lin-Gibson S, Schumacher GE, Flaim GM, Kohn J, Simon CG Jr (2008) X-ray imaging optimization of 3D tissue engineering scaffolds via combinatorial fabrication methods. *Biomaterials* 29:1901–1911
68. Kramer EJ (1983) Microscopic and molecular fundamentals of crazing. *Adv Polym Sci* 52/53:1–56
69. Lauterwasser BD, Kramer EJ (1979) Microscopic mechanisms and mechanics of craze growth and fracture. *Philos Mag A Phys Condens Matter Struct Defects Mech Prop* 39:469–495
70. Crosby AJ, Faselka MJ, Beers KL (2004) High-throughput craze studies in gradient thin films using ductile copper grids. *Macromolecules* 37:9968–9974
71. Stafford CM, Guo S, Harrison C, Chiang MYM (2005) Combinatorial and high-throughput measurements of the modulus of thin polymer films. *Rev Sci Instrum* 76:062207
72. Stafford CM, Harrison C, Beers KL, Karim A, Amis EJ, Vanlandingham MR, Kim HC, Volksen W, Miller RD, Simonyi EE (2004) A buckling-based metrology for measuring the elastic moduli of polymeric thin films. *Nat Mater* 3:545–550
73. Brandrup J, Immergut EH, Grulke EA (1999) *Polymer handbook*, 4th edn. Wiley, New York
74. Stafford CM, Vogt BD, Harrison C, Julthongpipit D, Huang R (2006) Elastic Moduli of ultrathin amorphous polymer films. *Macromolecules* 39:5095–5099
75. Nolte AJ, Cohen RE, Rubner MF (2006) A two-plate buckling technique for thin film modulus measurements: applications to polyelectrolyte multilayers. *Macromolecules* 39:4841–4847

76. Nolte AJ, Rubner MF, Cohen RE (2005) Determining the Young's modulus of polyelectrolyte multilayer films via stress-induced mechanical buckling instabilities. *Macromolecules* 38:5367–5370
77. Nolte AJ, Treat ND, Cohen RE, Rubner MF (2008) Effect of relative humidity on the Young's modulus of polyelectrolyte multilayer films and related nonionic polymers. *Macromolecules* 41:5793–5798
78. Huang H, Chung JY, Nolte AJ, Stafford CM (2007) Characterizing polymer brushes via surface wrinkling. *Chem Mater* 19:6555–6560
79. Khang DY, Xiao JL, Kocabas C, MacLaren S, Banks T, Jiang HQ, Huang YYG, Rogers JA (2008) Molecular scale buckling mechanics on individual aligned single-wall carbon nanotubes on elastomeric substrates. *Nano Lett* 8:124–130
80. Wilder EA, Guo S, Lin-Gibson S, Faselka MJ, Stafford CM (2006) Measuring the modulus of soft polymer networks via a buckling-based metrology. *Macromolecules* 39:4138–4143
81. Chisholm B, Potyrailo R, Cawse J, Shaffer R, Brennan M, Molaison C, Whisenhunt D, Flanagan B, Olson D, Akhave J, Saunders D, Mehrabi A, Licon M (2002) The development of combinatorial chemistry methods for coating development – I. Overview of the experimental factory. *Prog Org Coat* 45:313–321
82. Crosby AJ (2003) Combinatorial characterization of polymer adhesion. *J Mater Sci* 38:4439–4449
83. Chiche A, Zhang WH, Stafford CM, Karim A (2005) A new design for high-throughput peel tests: statistical analysis and example. *Meas Sci Technol* 16:183–190
84. McGuiggan PM, Chiche A, Filliben JJ, Phelan FR, Faselka MJ, Yarusso DJ (2006) High-throughput peel measurement of a pressure-sensitive adhesive. *Adhes Mag* 13:32–39
85. Grunlan JC, Holguin DL, Chuang HK, Perez I, Chavira A, Quilatan R, Akhave J, Mehrabi AR (2004) Combinatorial development of pressure-sensitive adhesives. *Macromol Rapid Commun* 25(1):286–291
86. Moon SH, Chiche A, Forster AM, Zhang WH, Stafford CM (2005) Evaluation of temperature-dependent adhesive performance via combinatorial probe tack measurements. *Rev Sci Instrum* 76:062210
87. Chisholm B, Potyrailo R, Shaffer R, Cawse J, Brennan M, Molaison C (2003) Combinatorial chemistry methods for coating development III. Development of a high-throughput screening method for abrasion resistance: correlation with conventional methods and the effects of abrasion mechanism. *Prog Org Coat* 47:112–119
88. Chisholm BJ, Potyrailo RA, Cawse JN, Shaffer RE, Brennan M, Molaison CA (2003) Combinatorial chemistry methods for coating development V. The importance of understanding process capability. *Prog Org Coat* 47:120–127
89. Shaffer EO, McGarry FJ, Hoang L (1996) Designing reliable polymer coatings. *Polym Eng Sci* 36:2375–2381
90. Chiang MYM, Wu WL, He JM, Amis EJ (2003) Combinatorial approach to the edge-delamination test for thin film reliability – concept and simulation. *Thin Solid Films* 437:197–203
91. Chiang MYM, Song R, Crosby AJ, Karim A, Chiang CK, Amis EJ (2005) Combinatorial approach to the edge-delamination test for thin film reliability – adaptability and variability. *Thin Solid Films* 476:379–385
92. Stafford CM, Kim JH, Kawaguchi D, Royston G, Chiang MYM (2006) Probing the interfacial adhesion strength in compositional libraries of epoxy films. *Mater Res Soc Symp Proc* 894:129–137
93. Johnson KL, Kendall K, Roberts AD (1971) Surface energy and contact of elastic solids. *Proc R Soc Lond A Math Phys Sci* 324:301
94. Crosby AJ, Karim A, Amis EJ (2003) Combinatorial investigations of interfacial failure. *J Polym Sci Part B Polym Phys* 41:883–891
95. Forster AM, Zhang WH, Crosby AJ, Stafford CM (2005) A multilens measurement platform for high-throughput adhesion measurements. *Meas Sci Technol* 16:81–89
96. Nolte AJ, Chung JY, Walker ML, Stafford CM (2009) In-situ adhesion measurements utilizing layer-by-layer functionalized surfaces. *ACS Appl Mater Interfaces* 1:373–380

97. Hessel V, Serra C, Loewe GH, Hadziioannou G (2005) Polymerizations in micro-structured reactors: overview. *Chem Ing Tech* 77:1693
98. Iwasaki T, Yoshida J (2005) Free radical polymerization in microreactors. Significant improvement in molecular weight distribution control. *Macromolecules* 38:1159–1163
99. Harrison C, Cabral J, Stafford CM, Karim A, Amis EJ (2004) A rapid prototyping technique for the fabrication of solvent-resistant structures. *J Micromech Microeng* 14:153–158
100. Cygan ZT, Cabral JT, Beers KL, Amis EJ (2005) Microfluidic platform for the generation of organic-phase microreactors. *Langmuir* 21:3629–3634
101. Chastek TQ, Iida K, Amis EJ, Fasolka MJ, Beers KL (2008) A microfluidic platform for integrated synthesis and dynamic light scattering measurement of block copolymer micelles. *Lab Chip* 8:950
102. Wu T, Mei Y, Cabral JT, Xu C, Beers KL (2004) A new synthetic method for controlled polymerization using a microfluidic system. *J Am Chem Soc* 126:7881
103. Wu T, Mei Y, Xu C, Byrd HCM, Beers KL (2005) Block copolymer PEO-b-PPMA synthesis using controlled radical polymerization on a chip. *Macromol Rapid Commun* 26:1037
104. Chastek TQ, Iida K, Amis EJ, Fasolka MJ, Beers KL (2008) A microfluidic platform for integrated synthesis and dynamic light scattering measurement of block copolymer micelles. *Lab Chip* 8:950–957
105. Iida K, Chastek TQ, Beers KL, Cavicchi KA, Chun J, Fasolka MJ (2009) Living anionic polymerization using a microfluidic reactor. *Lab Chip* 9:339–345
106. Chastek TQ, Beers KL, Amis EJ (2007) Miniaturized dynamic light scattering instrumentation for use in microfluidic applications. *Rev Sci Instrum* 78:072201
107. Jin F, Balasubramaniam R, Stebe KJ (2004) Surfactant adsorption to spherical particles: the intrinsic length-scale governing the shift from diffusion to kinetic-controlled mass transfer. *J Adhes* 80:773–796
108. Hudson SD, Cabral JT, Goodrum WJ, Beers KL, Amis EJ (2005) Microfluidic interfacial tensiometry. *Appl Phys Lett* 87:081905
109. Cabral JT, Hudson SD (2006) Microfluidic approach for rapid multicomponent interfacial tensiometry. *Lab Chip* 6:427–436